Available online at www.sciencedirect.com
SCIENCE DIRECT®
Journal of Computational Physics 198 (2004) 424–449
JOURNAL OF COMPUTATIONAL PHYSICS
www.elsevier.com/locate/jcp

Transport algorithms for partially ionized and unmagnetized plasmas

Thierry E. Magin [*,1], Gérard Degrez [1]

Department of Aeronautics and Aerospace, von Karman Institute for Fluid Dynamics, 72 Chaussée de Waterloo, B-1640 Rhode-Saint-Genèse, Belgium

Received 14 October 2003; received in revised form 16 January 2004; accepted 19 January 2004
Available online 21 February 2004

Abstract

A new formalism for the transport properties of partially ionized and unmagnetized plasmas is investigated from a computational point of view. Heavy particle transport expressions for shear viscosity, translational thermal conductivity, and thermal diffusion ratios are obtained from the solution of symmetric linear systems. Electron transport properties are also presented. A general Stefan–Maxwell equation and two approximate formulations deal with diffusion phenomenon. Well-posedness of the transport properties is established, provided that some conditions on the kinetic data are met. The mathematical structure of the transport matrices is readily used to build transport algorithms inspired by Ern and Giovangigli [J. Comput. Phys. 120 (1995) 105]. These algorithms rely either on a direct linear solver or on convergent iterative Krylov projection methods, such as the conjugate gradient. The Stefan–Maxwell matrix is singular and a mass conservation constraint completes the system of equations. A yet symmetric and non-singular Stefan–Maxwell matrix including the mass constraint is introduced for the direct method. A suitable projector associated with the singular form of the matrix is used for the iterative methods. An 11-species air mixture in local thermodynamic equilibrium at atmospheric pressure serves as benchmark to assess the physical model and numerical methods. Superiority of the conjugate gradient method with respect to the direct solver and approximate mixture rules found in the literature is demonstrated in terms of accuracy and computational cost.

AMS: 65F05; 65F010; 77D05

Keywords: Transport coefficients; Diffusion; Partially ionized mixtures; Unmagnetized plasmas; Iterative methods; Krylov subspaces

* Corresponding author.
E-mail addresses: magin@vki.ac.be (T.E. Magin), degrez@vki.ac.be (G. Degrez).
[1] Also at Université Libre de Bruxelles, Service de Mécanique des fluides, 50 Avenue F.D. Roosevelt, B-1050 Bruxelles, Belgium.

0021-9991/$ - see front matter
doi:10.1016/j.jcp.2004.01.012

1. Introduction

Transport phenomena in partially ionized and unmagnetized plasmas can be described by means of the kinetic theory of dilute gases. Transport fluxes are thoroughly derived for this type of plasma in a previous publication [1], principally based upon works of Kolesnikov [2] and Degond and Lucquin-Desreux [3]. Multicomponent transport coefficients are expressed as the solution of linear systems whose size is proportional to the number of species in the mixture. These systems are deduced from a symmetric formalism inspired by Chapman and Cowling [4] or Ferziger and Kaper [5], at variance with the non-symmetric approach of Hirschfelder et al. [6].

Evaluation of the multicomponent transport coefficients by direct inversion of these linear systems can be computationally expensive when the number of species becomes large. A symmetric formalism allows for the number of operations to be reduced by a factor of 2. However, the computational effort remains excessive for most fluid simulations. Approximate mixture rules constitute an alternative to evaluate at lower cost the multicomponent transport coefficients [7,8]. Unfortunately, these mixture rules are known to be inaccurate in the dissociation and ionization ranges [9–13]. Recently, another solution was proposed by Ern and Giovangigli [14] who developed low-cost accurate algorithms to provide the multicomponent transport properties of mixtures composed of neutral species. In the present work, these algorithms are adapted and applied to partially ionized and unmagnetized plasmas. The case of magnetized plasmas in thermal equilibrium is investigated by Giovangigli and Graille [15].

2. Transport fluxes

Our gas mixture is composed of N species referred to the set of indices $\mathscr{S} = \{1, \ldots, N\} = \mathscr{H} \cup \{\mathrm{e}\}$, where heavy particles are distinguished from electrons. Due to mass disparity, electrons and heavy particles exhibit distinct kinetic time scales. Consequently, small departures from thermal equilibrium may be envisaged. Electron translational temperature reads T_e and heavy particle translational temperature is for all $i \in \mathscr{H}$, $T_i = T_\mathrm{h}$, with $|T_\mathrm{e} - T_\mathrm{h}| \ll T_\mathrm{e} \sim T_\mathrm{h}$. The Knudsen number is assumed to be small, the gas is collision-dominated. The Hall parameter of electrons is smaller than the Knudsen number. Thus, the magnetic field influence on transport properties remains negligible, the plasma is unmagnetized. The Debye length is considered to be smaller than a reference length in the flow, the plasma is quasi-neutral. The influence of chemical reactions on transport phenomena is neglected. The validity of these assumptions is discussed in [1].

2.1. Governing equations

The Navier–Stokes equations for chemically reacting flows are presented neglecting the internal energy of atoms and polyatomic molecules. A general treatment of the internal energy requires specific energy relaxation models between the various energy modes. This is not the object of the present research. Hence, the Navier–Stokes equations read

$$\partial_t(\rho_i) + \nabla \cdot (\rho_i \mathbf{v}) + \nabla \cdot (\rho_i \mathbf{V}_i) = \omega_i, \quad i \in \mathscr{S}, \tag{1a}$$

$$\partial_t(\rho) + \nabla \cdot (\rho \mathbf{v}) = 0, \tag{1b}$$

$$\partial_t(\rho \mathbf{v}) + \nabla \cdot (\rho \mathbf{v} \otimes \mathbf{v}) + \nabla \cdot \mathsf{P} = \mathbf{j} \times \mathbf{B}, \tag{1c}$$

$$\partial_t(\rho_e e_e) + \nabla\cdot(\rho_e e_e \mathbf{v}) + \nabla\cdot(\mathbf{q}_e) = -\rho_e \mathbf{V}_e \cdot \frac{\mathrm{d}}{\mathrm{d}t}\mathbf{v} - p_e : \nabla\mathbf{v} + \mathbf{j}_e \cdot \mathbf{E}' + \Delta E_e^0, \tag{1d}$$

$$\partial_t(\rho e) + \nabla\cdot(\rho e \mathbf{v}) + \nabla\cdot(\mathbf{q}_h + \mathbf{q}_e) = -\mathsf{P} : \nabla\mathbf{v} + \mathbf{j}\cdot\mathbf{E}', \tag{1e}$$

where ρ_i is the species mass density, $\rho = \sum_{j\in\mathscr{S}} \rho_j$ the mixture mass density, $\mathbf{v}$ the hydrodynamic velocity, ω_i the species mass production rate, $\rho_i e_i = \frac{3}{2} n_i k_B T_i$ the species translational energy, $\rho e = \sum_{j\in\mathscr{S}} \rho_j e_j$ the mixture translational energy, and p_i the partial pressure. The transport fluxes are the diffusion velocities $\mathbf{V}_i$, shear stress P, heavy particle heat flux $\mathbf{q}_h$, and electron heat flux $\mathbf{q}_e$. Symbol $\mathrm{d}/\mathrm{d}t = \partial_t + \mathbf{v}\cdot\nabla$ stands for the material derivative. The conduction current of species i is given by the flux of charge $\mathbf{j}_i = n_i q_i \mathbf{V}_i$, where n_i and q_i are the species number density and charge. The mixture conduction current reads $\mathbf{j} = \sum_{j\in\mathscr{S}} \mathbf{j}_j$. The electric field in the hydrodynamic velocity frame reads $\mathbf{E}' = \mathbf{E} + \mathbf{v}\times\mathbf{B}$, where $\mathbf{E}$ is the electric field and $\mathbf{B}$ the magnetic field. The energy exchanged by elastic collisions between electrons and heavy particles ΔE_e^0 is given in Appendix B.

2.2. Kinetic expressions

The solution of the Boltzmann equation for dilute gases allows for the transport fluxes of a partially ionized plasma to be computed. The plasma parameter is proportional to the number of electrons in a sphere of radius equal to the Debye length. This number is assumed to be sufficiently large such that charged particle interactions can be treated as binary collisions with a Debye–Hückel screening of the Coulomb potential. Furthermore, ionized gases composed of electrons and heavy particles require a special treatment due to a mass disparity between both species. In [1], a dimensional analysis of the Boltzmann equation exhibits different kinetic time scales for electrons and heavy particles. Their translational temperatures may differ but their hydrodynamic velocity is supposed to be identical. At the hydrodynamic time scale, the energy exchanged between electrons and heavy particles tends to equalize both temperatures. A perturbative Chapman–Enskog method, modified to deal with mass disparity and thermal non-equilibrium, supplies with integral equations. A spectral Galerkin projection using Laguerre–Sonine polynomials yields transport systems. In this section, final expressions of the transport fluxes are presented in terms of reduced collision integrals (see their definition in Appendix A), more suitable for applications than the collision integrals of [1]. Transport matrices are explicited in Appendix C. The internal energy is not taken into account. The influence of the internal degrees of freedom on transport phenomena is addressed in various specialized publications cited in the general reference [5]. However, a rigorous treatment of the internal energy leads to transport collision integrals difficult to estimate with accuracy in high-temperature plasmas. Capitelli et al. [16,17] have recently assessed the role of electronically excited states on the viscosity and reactive thermal conductivity for a hydrogen plasma in the temperature range 10,000–25,000 K by computing the adequate resonant charge and excitation transfer cross-sections. In Section 4, a passive transport of the internal energy has been retained instead, neglecting inelastic collisions.

2.2.1. Shear stress

Shear stress reads

$$\mathsf{P} = p\mathsf{I} - \eta[\nabla\mathbf{v} + (\nabla\mathbf{v})^{\mathrm{T}}] + \tfrac{2}{3}\eta\nabla\cdot\mathbf{v}\mathsf{I}, \tag{2}$$

where $p = \sum_{j\in\mathscr{S}} p_j$ is the pressure of the mixture. Symbol I stands for the identity tensor. The shear viscosity η is given in the first Laguerre–Sonine approximation denoted by $\eta(1)$

$$\sum_{j\in\mathscr{H}} G_{ij}^{\eta}\alpha_j^{\eta} = x_i, \quad i\in\mathscr{H}, \tag{3a}$$

$$\eta(1) = \sum_{j\in\mathscr{H}} \alpha_j^{\eta} x_j, \tag{3b}$$

where x_i is the mole fraction of species i. Electrons do not contribute to the viscous shear stress.

2.2.2. Heavy particle heat flux

The heavy particle heat flux is expressed by

$$\mathbf{q}_{\mathrm{h}} = \sum_{j\in\mathscr{H}} \rho_j h_j \mathbf{V}_j + n k_{\mathrm{B}} T_{\mathrm{h}} \sum_{j\in\mathscr{H}} k_{\mathrm{T}j}^{\mathrm{h}} \mathbf{V}_j - \lambda_{\mathrm{h}} \nabla T_{\mathrm{h}}, \tag{4}$$

where n and k_{B} are the mixture number density and Boltzmann constant. Species enthalpies read

$$h_i = h_{\mathrm{T}i} + h_{\mathrm{F}i}, \quad i \in \mathscr{H}, \tag{5}$$

where $h_{\mathrm{T}i}$ is the translational species enthalpy, evaluated at the translational temperature T_{h}. The chemical reaction contribution is included by means of the formation enthalpy $h_{\mathrm{F}i}$. The translational thermal conductivity λ_{h} of heavy particles is given in the second Laguerre–Sonine approximation denoted by $\lambda_{\mathrm{h}}(2)$

$$\sum_{j\in\mathscr{H}} G_{ij}^{\lambda_{\mathrm{h}}} \alpha_j^{\lambda_{\mathrm{h}}} = x_i, \quad i \in \mathscr{H}, \tag{6a}$$

$$\lambda_{\mathrm{h}}(2) = \sum_{j\in\mathscr{H}} \alpha_j^{\lambda_{\mathrm{h}}} x_j. \tag{6b}$$

Heavy particle thermal diffusion ratios $k_{\mathrm{T}j}^{\mathrm{h}}$ are then obtained as follows:

$$k_{\mathrm{T}i}^{\mathrm{h}}(2) = \frac{5}{2} \sum_{j\in\mathscr{H}} \Lambda_{ij}^{01} \alpha_j^{\lambda_{\mathrm{h}}}, \quad i \in \mathscr{H}, \tag{7}$$

where $\sum_{j\in\mathscr{H}} k_{\mathrm{T}j}^{\mathrm{h}} = 0$ and $k_{\mathrm{T_e}}^{\mathrm{h}} = 0$. The translational thermal conductivity and thermal diffusion ratios of heavy particles do not depend on electrons.

2.2.3. Electron heat flux

The electron heat flux is expressed by

$$\mathbf{q}_{\mathrm{e}} = \rho_{\mathrm{e}} h_{\mathrm{e}} \mathbf{V}_{\mathrm{e}} + n k_{\mathrm{B}} T_{\mathrm{h}} \sum_{j\in\mathscr{S}} k_{\mathrm{T}j}^{\mathrm{e}} \mathbf{V}_j - \lambda_{\mathrm{e}} \nabla T_{\mathrm{e}}, \tag{8}$$

where the electron enthalpy is composed of translational and formation contributions

$$h_{\mathrm{e}} = h_{\mathrm{T_e}} + h_{\mathrm{F_e}}. \tag{9}$$

Translational enthalpy is evaluated at the electron translational temperature T_{e}. The electron thermal conductivity λ_{e} reads in the second and third Laguerre–Sonine approximations

$$\lambda_{\mathrm{e}}(2) = \frac{x_{\mathrm{e}}^2}{\Lambda_{\mathrm{ee}}^{11}}, \tag{10a}$$

$$\lambda_{\mathrm{e}}(3) = \frac{x_{\mathrm{e}}^2 \Lambda_{\mathrm{ee}}^{22}}{\Lambda_{\mathrm{ee}}^{11}\Lambda_{\mathrm{ee}}^{22} - \left(\Lambda_{\mathrm{ee}}^{12}\right)^2}. \tag{10b}$$

Electron thermal diffusion ratios $k^{\mathrm{e}}_{\mathrm{T}i}$ are obtained from

$$k^{\mathrm{e}}_{\mathrm{T}i}(2) = \frac{5}{2}\frac{T_{\mathrm{e}}}{T_{\mathrm{h}}}x_{\mathrm{e}}\frac{\Lambda^{01}_{i\mathrm{e}}}{\Lambda^{11}_{\mathrm{ee}}}, \tag{11a}$$

$$k^{\mathrm{e}}_{\mathrm{T}i}(3) = \frac{5}{2}\frac{T_{\mathrm{e}}}{T_{\mathrm{h}}}x_{\mathrm{e}}\frac{\Lambda^{01}_{i\mathrm{e}}\Lambda^{22}_{\mathrm{ee}} - \Lambda^{02}_{i\mathrm{e}}\Lambda^{12}_{\mathrm{ee}}}{\Lambda^{11}_{\mathrm{ee}}\Lambda^{22}_{\mathrm{ee}} - \left(\Lambda^{12}_{\mathrm{ee}}\right)^2}, \tag{11b}$$

where $i \in \mathscr{S}$ and $\sum_{j\in\mathscr{H}} k^{\mathrm{e}}_{\mathrm{T}j} + k^{\mathrm{e}}_{\mathrm{T_e}} T_{\mathrm{e}}/T_{\mathrm{h}} = 0$.

2.2.4. Diffusion velocities

The diffusion velocity of species i reads

$$\mathbf{V}_i = -\sum_{j\in\mathscr{S}} D_{ij}\left(\mathbf{d}_j + k^{\mathrm{h}}_{\mathrm{T}j}\nabla\ln T_{\mathrm{h}} + k^{\mathrm{e}}_{\mathrm{T}j}\nabla\ln T_{\mathrm{e}}\right), \tag{12}$$

where driving forces are defined as

$$\mathbf{d}_i = \frac{\nabla p_i}{nk_{\mathrm{B}}T_{\mathrm{h}}} - \frac{y_i p}{nk_{\mathrm{B}}T_{\mathrm{h}}}\nabla\ln p - \kappa_i\mathbf{E}. \tag{13}$$

Symbol y_i is the species mass fraction. Expression κ_i stands for $x_i q_i/(k_{\mathrm{B}}T_{\mathrm{h}}) - y_i q/(k_{\mathrm{B}}T_{\mathrm{h}})$, where $q = \sum_{j\in\mathscr{S}} x_j q_j$ is the mixture charge. Mass conservation is expressed by the constraint

$$\sum_{j\in\mathscr{S}} \mathscr{G}^{\mathbf{V}}_j \mathbf{V}_j = 0, \tag{14}$$

where $\mathscr{G}^{\mathbf{V}}_i = y_i,\ i \in \mathscr{S}$. Quantities $\mathbf{d}_i$ and κ_i are not linearly independent, $\sum_{j\in\mathscr{S}}\mathbf{d}_j = 0$ and $\sum_{j\in\mathscr{S}}\kappa_j = 0$. Diffusion coefficients D_{ij} determine the diffusion velocities given in Eq. (12). Equivalently, the diffusion velocities are found to be solution of a generalized Stefan–Maxwell equation

$$\sum_{j\in\mathscr{S}} G^{\mathbf{V}}_{ij}\mathbf{V}_j - \kappa_i\mathbf{E} = -\mathbf{d}'_i, \quad i \in \mathscr{H}, \tag{15a}$$

$$\sum_{j\in\mathscr{S}} G^{\mathbf{V}}_{\mathrm{e}j}\mathbf{V}_j - \kappa_{\mathrm{e}}\frac{T_{\mathrm{h}}}{T_{\mathrm{e}}}\mathbf{E} = -\frac{T_{\mathrm{h}}}{T_{\mathrm{e}}}\mathbf{d}'_{\mathrm{e}}. \tag{15b}$$

Modified driving forces are introduced

$$\mathbf{d}'_i = \frac{\nabla p_i}{nk_{\mathrm{B}}T_{\mathrm{h}}} - \frac{y_i p}{nk_{\mathrm{B}}T_{\mathrm{h}}}\nabla\ln p + k^{\mathrm{h}}_{\mathrm{T}i}\nabla\ln T_{\mathrm{h}} + k^{\mathrm{e}}_{\mathrm{T}i}\frac{T_i}{T_{\mathrm{e}}}\nabla\ln T_{\mathrm{e}}, \tag{16}$$

with $\sum_{j\in\mathscr{S}}\mathbf{d}'_j = 0$. The Stefan–Maxwell equation keeps the same structure independently of the Laguerre–Sonine approximation order.

Approximations of the generalized Stefan–Maxwell equation are derived in [1]. Assuming that for all $i \in \mathscr{H}$, there exists $j \in \mathscr{H},\ j \neq i$, such that $x_{\mathrm{e}}/\mathscr{D}_{i\mathrm{e}} \ll x_j/\mathscr{D}_{ij}$, Kolesnikov's model [18] is retrieved

$$\sum_{j\in\mathscr{S}} \tilde{G}^{\mathbf{V}}_{ij}\mathbf{V}_j - \kappa_i\mathbf{E} = -\mathbf{d}'_i, \quad i \in \mathscr{H}, \tag{17a}$$

$$\tilde{G}^{\mathrm{V}}_{\mathrm{ee}}\mathbf{V}_{\mathrm{e}} - \kappa_{\mathrm{e}}\frac{T_{\mathrm{h}}}{T_{\mathrm{e}}}\mathbf{E} = -\frac{T_{\mathrm{h}}}{T_{\mathrm{e}}}\mathbf{d}'_{\mathrm{e}}. \tag{17b}$$

Seeing that $\mathscr{D}_{i\mathrm{e}} \gg \mathscr{D}_{ij}$, for all $i,j \in \mathscr{H}$, the hypothesis on Kolesnikov's model is always satisfied for partially ionized plasmas. Assuming further that for all $i \in \mathscr{H}$, there exists $j \in \mathscr{H}$, $j \neq i$, such that $x_{\mathrm{e}}V_{\mathrm{e}}/\mathscr{D}_{i\mathrm{e}} \ll x_jV_j/\mathscr{D}_{ij}$ or such that $x_{\mathrm{e}}V_{\mathrm{e}}/\mathscr{D}_{i\mathrm{e}} \ll x_jV_i/\mathscr{D}_{ij}$, a generalization of Ramshaw and Chang's hydrodynamic model [19] is obtained. The electric field is given by $\mathbf{E} = \mathbf{d}'_{\mathrm{e}}/\kappa_{\mathrm{e}}$, and the diffusion velocities of heavy particles are determined from

$$\sum_{j\in\mathscr{H}} \hat{G}^{\mathrm{V}}_{ij}\mathbf{V}_j = -\mathbf{d}'_i + \frac{\kappa_i}{\kappa_{\mathrm{e}}}\mathbf{d}'_{\mathrm{e}}, \quad i \in \mathscr{H}. \tag{18}$$

Eq. (18) relies on a strong hypothesis. Therefore, its validity domain is restricted.

2.2.5. Conduction current

Using Eq. (12), Ohm's law for unmagnetized plasmas is obtained

$$\mathbf{j} = \sigma\mathbf{E} - \sum_{i,j\in\mathscr{S}} n_iq_iD_{ij}\left(\frac{\nabla p_j}{nk_{\mathrm{B}}T_{\mathrm{h}}} - \frac{y_jp}{nk_{\mathrm{B}}T_{\mathrm{h}}}\nabla\ln p + k^{\mathrm{h}}_{\mathrm{T}j}\nabla\ln T_{\mathrm{h}} + k^{\mathrm{e}}_{\mathrm{T}j}\nabla\ln T_{\mathrm{e}}\right), \tag{19}$$

where the electrical conductivity reads $\sigma = \sum_{i,j\in\mathscr{S}} n_iq_iD_{ij}\kappa_j$. Current flows due to an electric field, concentration gradients, pressure gradients, and thermal diffusion. The conduction current can be alternately derived from the Stefan–Maxwell equations (15) or (17), supplied with the mass constraint given by Eq. (14). The order of magnitude of the electron diffusion velocity with respect to that of heavy particles depends on the specific electric field and driving forces. Two particular cases often encountered in practice are now examined.

First, in the absence of any spatial gradients, the only driving force is the electric field. It can be shown that electrons diffuse faster than heavy particles for a quasi-neutral plasma, $V_{\mathrm{e}} \gg V_i$, $i \in \mathscr{H}$. Hence, the main contribution to the conduction current comes from electrons, $\mathbf{j} \sim \mathbf{j}_{\mathrm{e}} = n_{\mathrm{e}}q_{\mathrm{e}}\mathbf{V}_{\mathrm{e}}$. In this case, the electrical conductivity is simply given by $\sigma_{\mathrm{e}} = n_{\mathrm{e}}q_{\mathrm{e}}D_{\mathrm{ee}}\kappa_{\mathrm{e}}$. Equivalently, the non-symmetric form of the Stefan–Maxwell equation (17b) yields $\sigma_{\mathrm{e}} = n_{\mathrm{e}}q_{\mathrm{e}}\kappa_{\mathrm{e}}T_{\mathrm{h}}/(T_{\mathrm{e}}\tilde{G}^{\mathrm{V}}_{\mathrm{ee}})$. After some algebra, and using the expression of $\tilde{G}^{\mathrm{V}}_{\mathrm{ee}}$ presented in Appendix C, the electrical conductivity reads in the first and second Laguerre–Sonine approximations

$$\sigma_{\mathrm{e}}(1) = \frac{4}{25}\frac{(x_{\mathrm{e}}q_{\mathrm{e}})^2}{k_{\mathrm{B}}^2T_{\mathrm{e}}}\frac{1}{\Lambda^{00}_{\mathrm{ee}}}, \tag{20a}$$

$$\sigma_{\mathrm{e}}(2) = \frac{4}{25}\frac{(x_{\mathrm{e}}q_{\mathrm{e}})^2}{k_{\mathrm{B}}^2T_{\mathrm{e}}}\frac{1}{\Lambda^{00}_{\mathrm{ee}} - \left(\Lambda^{01}_{\mathrm{ee}}\right)^2/\Lambda^{11}_{\mathrm{ee}}}. \tag{20b}$$

Expressions given in Eq. (20) are shown to be identical to those introduced by Devoto [20]. Notice that Eq. (18) is not valid in this situation.

Second, the electric field is sometimes determined from the ambipolar assumption $\sum_{j\in\mathscr{S}} x_jq_j\mathbf{V}_j = 0$, i.e., the conduction current is assumed to be zero. The ambipolar assumption combined to the mass constraint [see Eq. (14)] yields the closure

$$\sum_{j\in\mathscr{S}} \kappa_j\mathbf{V}_j = 0. \tag{21}$$

Eq. (21) is preferred to the ambipolar constraint in order to keep a symmetric formulation in thermal equilibrium when it is used with the Stefan–Maxwell equation (15) and the mass conservation constraint given in Eq. (14). The approximation given in Eq. (17) can also be substituted to Eq. (15). Furthermore, due to the plasma quasi-neutrality and ambipolar assumption, diffusion velocity of electrons is of the same order of magnitude as that of ions. Consequently, Eq. (18) is always valid for partially ionized plasmas with an ambipolar electric field. The mass conservation reads

$$\sum_{j\in\mathscr{H}} \hat{\mathscr{G}}_j^{\mathbf{V}} \mathbf{V}_j = 0, \tag{22}$$

where $\hat{\mathscr{G}}_i^{\mathbf{V}} = y_i,\ i \in \mathscr{H}$. The electron diffusion velocity is obtained from $\mathbf{V}_\mathrm{e} = -\sum_{j\in\mathscr{H}} x_j q_j \mathbf{V}_j/(x_\mathrm{e} q_\mathrm{e})$.

2.3. Mathematical properties

2.3.1. Heavy particle systems

In Eqs. (3) and (6), transport systems for the shear viscosity and translational thermal conductivity of heavy particles take the form $G^\mu \alpha^\mu = \beta^\mu$, where the symmetric matrix $G^\mu \in \mathbb{R}^{N-1,N-1}$ and vectors $\alpha^\mu, \beta^\mu \in \mathbb{R}^{N-1}$ ($\beta_i^\mu = x_i,\ i \in \mathscr{H}$). Transport coefficients $\mu = \eta$ and $\mu = \lambda_\mathrm{h}$ are then expressed as a scalar product $\mu = (\alpha^\mu)^\mathrm{T} \beta^\mu$. Electrons do not contribute to these properties and systems correspond to a gas only composed of heavy particles. Consequently, mathematical properties established for shear viscosity and translational thermal conductivity of mixtures of neutral species can be directly applied to ionized plasmas, provided that inelastic collisions are neglected. The following proposition is taken from [21].

Proposition 1. *Let A_{ij}^*, B_{ij}^*, and $\mathscr{D}_{ij}$, $i,j \in \mathscr{H},\ i \neq j$, be symmetric positive coefficients such that $B_{ij}^* < 25/12$, let $\eta_i,\ i \in \mathscr{H}$, be positive coefficients and assume that $x_i > 0,\ i \in \mathscr{H}$. Then, the matrices G^η, G^{λ_h}, $\mathrm{diag}(G^\eta)$, and $\mathrm{diag}(G^{\lambda_\mathrm{h}})$ are symmetric positive definite.*

A diagonal matrix based upon the matrix $A \in \mathbb{R}^{n,n}$ is defined as $\mathrm{diag}(A) = (A_{ij}\delta_{ij})_{i,j\in\{1,\ldots,n\}}$, where δ_{ij} is the Kronecker symbol. Positivity of the matrix G^μ ensures well-posedness of the system $G^\mu \alpha^\mu = \beta^\mu$ and supplies with positive transport properties $\mu = (\alpha^\mu)^\mathrm{T} \beta^\mu$, i.e., $\eta > 0$ and $\lambda_\mathrm{h} > 0$. Proposition 1 remains valid for positive mole fractions of heavy particles. In particular, we have $\sum_{j\in\mathscr{H}} x_j = 1 - x_\mathrm{e}$. Furthermore, hypothesis of positive mole fractions is always satisfied from a physical standpoint. Nevertheless, from a computational point of view, Ern and Giovangigli [21] have shown smoothness of the shear viscosity and translational thermal conductivity when some mole fractions become arbitrarily small. Henceforth, transport properties are evaluated in practice by first adding to all the species mole fractions a small number to avoid any problems in the numerical method.

In Eq. (18), matrix $\hat{G}^{\mathbf{V}} \in \mathbb{R}^{N-1,N-1}$ depends only on heavy particles. This matrix is singular, as shown in the following proposition.

Proposition 2. *Let $\mathscr{D}_{ij}$ and φ_{ij}, $i,j \in \mathscr{H}$, $i \neq j$, be symmetric positive coefficients such that $\varphi_{ij} > -1$ and assume that $x_i > 0,\ i \in \mathscr{H}$. Then, the matrix $\hat{G}^{\mathbf{V}}$ is symmetric positive semi-definite and $\mathrm{diag}(\hat{G}^{\mathbf{V}})$ is positive definite. Furthermore, the nullspace of $\hat{G}^{\mathbf{V}}$ is spanned by the vector $\hat{\mathscr{R}}^{\mathbf{V}}$, where $\hat{\mathscr{R}}_i^{\mathbf{V}} = 1,\ i \in \mathscr{H}$.*

Proof. An explicit calculation yields for $\alpha \in \mathbb{R}^{N-1},\ \alpha \neq 0$

$$\alpha^\mathrm{T} \hat{G}^{\mathbf{V}} \alpha = \frac{1}{2} \sum_{\substack{i,j\in\mathscr{H} \\ i\neq j}} \frac{x_i x_j}{\mathscr{D}_{ij}} (1 + \varphi_{ij})(\alpha_i - \alpha_j)^2 \geqslant 0, \quad = 0 \text{ if and only if } \alpha_i = c,\ i \in \mathscr{H},\ c \in \mathbb{R} \setminus \{0\}.$$

The nullspace is determined from the property $\alpha^{\mathrm{T}} G\alpha = 0 \Longleftrightarrow G\alpha = 0$, for G symmetric positive semi-definite. Positivity of $\mathrm{diag}(\hat{G}^{\mathbf{V}})$ is trivial to establish. □

Following [21], the constraint vector $\hat{\mathscr{G}}^{\mathbf{V}} \in \mathbb{R}^{N-1}$ of Eq. (22) allows for a non-singular matrix $\hat{G}^{\mathbf{V}} + a\hat{\mathscr{G}}^{\mathbf{V}} \otimes \hat{\mathscr{G}}^{\mathbf{V}}$ to be introduced, where $a \in \mathbb{R} \setminus \{0\}$. The following lemma is an adaptation for a matrix possibly non-symmetric and with a one-dimensional nullspace of a proposition found in [22]. It can be particularized to a symmetric positive semi-definite matrix such as $\hat{G}^{\mathbf{V}}$. The non-symmetry property is necessary for the matrix $\tilde{G}^{\mathbf{V}}$.

Lemma 3. *Let $G \in \mathbb{R}^{n,n}$ be a matrix such that the nullspaces of G and G^{T} are, respectively, spanned by the vectors $\mathscr{R} \in \mathbb{R}^n$ and $\mathscr{L} \in \mathbb{R}^n$. Let $\mathscr{G} \in \mathbb{R}^n$ be a vector such that $\mathscr{R}^{\mathrm{T}}\mathscr{G} \neq 0$ and $\mathscr{L}^{\mathrm{T}}\mathscr{G} \neq 0$. Then, the oblique projector P onto the hyperplane $\perp \mathscr{G}$ along $\mathscr{R}$ reads $P_{ij} = \delta_{ij} - \mathscr{R}_i\mathscr{G}_j/(\mathscr{R}^{\mathrm{T}}\mathscr{G})$. Furthermore, the matrix $G + a\mathscr{G} \otimes \mathscr{G}$, where $a \in \mathbb{R} \setminus \{0\}$, is non-singular. For a vector $\beta \in \mathbb{R}^n$ and in the range $R(G)$ of G, the solution α of the system $(G + a\mathscr{G} \otimes \mathscr{G})\alpha = \beta$ satisfies the system $G\alpha = \beta$ and the constraint $\mathscr{G}^{\mathrm{T}}\alpha = 0$.*

Proof. The matrix $G + a\mathscr{G} \otimes \mathscr{G}$ is non-singular, otherwise there exists a vector $\alpha \in \mathbb{R}^n$, $\alpha \neq 0$, such that $(G + a\mathscr{G} \otimes \mathscr{G})\alpha = 0$. Multiplying this expression by $\mathscr{L}^{\mathrm{T}}$, one gets $\mathscr{G}^{\mathrm{T}}\alpha = 0$, seeing that $\mathscr{L}^{\mathrm{T}}G = 0$ and $\mathscr{L}^{\mathrm{T}}\mathscr{G} \neq 0$. Therefore, $\alpha \in N(G)$. This is in contradiction with the hypothesis $\mathscr{R}^{\mathrm{T}}\mathscr{G} \neq 0$. The rest of the proof, straightforward, is omitted. □

Lemma 3 ensures well-posedness of the Stefan–Maxwell equation (18) with the mass constraint given in Eq. (22).

2.3.2. Electron systems

Properties of the scalars $\Lambda^{00}_{\mathrm{ee}}$ and $\Lambda^{11}_{\mathrm{ee}}$ are deduced from their definition (see Appendix C).

Proposition 4. *Let $\bar{Q}^{(1,1)}_{i\mathrm{e}}$, $\bar{Q}^{(1,2)}_{i\mathrm{e}}$, $\bar{Q}^{(1,3)}_{i\mathrm{e}}$, $i \in \mathscr{H}$, and $\bar{Q}^{(2,2)}_{\mathrm{ee}}$ be positive coefficients such that $5\bar{Q}^{(1,2)}_{i\mathrm{e}} - 4\bar{Q}^{(1,3)}_{i\mathrm{e}} < 25\bar{Q}^{(1,1)}_{i\mathrm{e}}/12$ and assume that $x_i > 0$, $i \in \mathscr{S}$. Then, the scalars $\Lambda^{00}_{\mathrm{ee}}$ and $\Lambda^{11}_{\mathrm{ee}}$ are positive.*

This proposition supplies with well-posedness and positivity of the electron thermal conductivity $\lambda_{\mathrm{e}}(2)$ and electrical conductivity $\sigma_{\mathrm{e}}(1)$. Conditions on reduced collision integrals for higher Laguerre–Sonine approximations are not detailed in this work.

2.3.3. Electron-heavy particle systems

In the Stefan–Maxwell equations (15) and (17), matrices $G^{\mathbf{V}}$ and $\tilde{G}^{\mathbf{V}} \in \mathbb{R}^{N,N}$ include both electron and heavy particle contributions.

Proposition 5. *Let $\mathscr{D}_{ij}$ and φ_{ij}, $i, j \in \mathscr{S}$, $i \neq j$, be symmetric positive coefficients such that $\varphi_{ij} > -1$ and assume that $x_i > 0$, $i \in \mathscr{S}$. Then, the matrix $G^{\mathbf{V}}$ is symmetric positive semi-definite and $\mathrm{diag}(G^{\mathbf{V}})$ is positive definite. Furthermore, the nullspace of $G^{\mathbf{V}}$ is spanned by the vector $\mathscr{R}^{\mathbf{V}}$, where $\mathscr{R}^{\mathbf{V}}_i = 1$, $i \in \mathscr{H}$, and $\mathscr{R}^{\mathbf{V}}_{\mathrm{e}} = T_{\mathrm{e}}/T_{\mathrm{h}}$.*

Proof. The proof is identical to that of Proposition 2. An explicit calculation yields for $\alpha \in \mathbb{R}^N, \alpha \neq 0$

$$\begin{aligned}\alpha^{\mathrm{T}} G^{\mathbf{V}} \alpha &= \frac{1}{2} \sum_{\substack{i,j \in \mathscr{H} \\ i \neq j}} \frac{x_i x_j}{\mathscr{D}_{ij}} \left(1 + \varphi_{ij}\right)\left(\alpha_i - \alpha_j\right)^2 + \frac{1}{2} \sum_{j \in \mathscr{H}} \frac{x_{\mathrm{e}} x_j}{\mathscr{D}_{\mathrm{e}j}} \left(1 + \varphi_{\mathrm{e}j}\right)\left(\alpha_{\mathrm{e}} - \frac{T_{\mathrm{e}}}{T_{\mathrm{h}}}\alpha_j\right)^2 \geqslant 0, \\ &= 0 \quad \text{if and only if } \alpha_i = c,\ i \in \mathscr{H},\ c \in \mathbb{R} \setminus \{0\} \text{ and } \alpha_{\mathrm{e}} = cT_{\mathrm{e}}/T_{\mathrm{h}}.\end{aligned}$$

Positivity of $\mathrm{diag}(G^{\mathbf{V}})$ is readily deduced from its definition. □

Proposition 6. *Let* $\mathscr{D}_{ij}$ *and* φ_{ij}, $i,j \in \mathscr{S}$, $i \neq j$, *be symmetric positive coefficients such that* $\varphi_{ij} > -1$ *and assume that* $x_i > 0$, $i \in \mathscr{S}$. *Then, the matrix* $\tilde{G}^{\mathbf{V}} \in \mathbb{R}^{N,N}$ *is non-symmetric and indefinite, and the matrix* $\mathrm{diag}(\tilde{G}^{\mathbf{V}})$ *is positive definite. Furthermore, the nullspaces of* $\tilde{G}^{\mathbf{V}}$ *and* $(\tilde{G}^{\mathbf{V}})^{\mathrm{T}}$ *are, respectively, spanned by the vectors* $\tilde{\mathscr{R}}^{\mathbf{V}}$ *and* $\tilde{\mathscr{L}}^{\mathbf{V}}$, *where* $\tilde{\mathscr{R}}^{\mathbf{V}}_i = \tilde{\mathscr{L}}^{\mathbf{V}}_i = 1$, $i \in \mathscr{H}$, $\tilde{\mathscr{R}}^{\mathbf{V}}_{\mathrm{e}} = 0$, *and* $\tilde{\mathscr{L}}^{\mathbf{V}}_{\mathrm{e}} = T_{\mathrm{e}}/T_{\mathrm{h}}$.

Proof. As usual, an explicit calculation yields for $\alpha \in \mathbb{R}^N$, $\alpha \neq 0$

$$\alpha^{\mathrm{T}}\tilde{G}^{\mathbf{V}}\alpha = \frac{1}{2}\sum_{\substack{i,j\in\mathscr{H}\\ i\neq j}} \frac{x_i x_j}{\mathscr{D}_{ij}}\left(1+\varphi_{ij}\right)\left(\alpha_i-\alpha_j\right)^2 + \frac{1}{2}\sum_{j\in\mathscr{H}} \frac{x_{\mathrm{e}} x_j}{\mathscr{D}_{\mathrm{e}j}}\left(1+\varphi_{\mathrm{e}j}\right)\left(\alpha_{\mathrm{e}}^2 - \frac{T_{\mathrm{e}}}{T_{\mathrm{h}}}\alpha_j\alpha_{\mathrm{e}}\right),$$

showing that $\tilde{G}^{\mathbf{V}}$ is indefinite. Positivity of $\mathrm{diag}(\tilde{G}^{\mathbf{V}})$ comes from its definition. The vector $\tilde{\mathscr{R}}^{\mathbf{V}} \in N(\tilde{G}^{\mathbf{V}})$ and the vector $\tilde{\mathscr{L}}^{\mathbf{V}} \in N[(\tilde{G}^{\mathbf{V}})^{\mathrm{T}}]$. Since the line $\tilde{G}^{\mathbf{V}}_{\mathrm{e}i}$, $i \in \mathscr{S}$, has only zero entries except $\tilde{G}^{\mathbf{V}}_{\mathrm{ee}}$, a vector $\alpha \in N(\tilde{G}^{\mathbf{V}})$ is such that $\alpha_{\mathrm{e}} = 0$. Hence, $(\alpha_i)_{i\in\mathscr{H}} \in [N(\tilde{G}^{\mathbf{V}}_{ij})]_{i,j\in\mathscr{H}}$. From the relation $\tilde{G}^{\mathbf{V}}_{ij} = \hat{G}^{\mathbf{V}}_{ij}$, $i,j \in \mathscr{H}$, and Proposition 2, one deduces that $N(\tilde{G}^{\mathbf{V}})$ is one-dimensional. □

Following [21], the constraint vector $\mathscr{G}^{\mathbf{V}} \in \mathbb{R}^N$ given in Eq. (14) allows for non-singular matrices $G^{\mathbf{V}} + a\mathscr{G}^{\mathbf{V}} \otimes \mathscr{G}^{\mathbf{V}}$ and $\tilde{G}^{\mathbf{V}} + a\mathscr{G}^{\mathbf{V}} \otimes \mathscr{G}^{\mathbf{V}}$ to be introduced, where $a \in \mathbb{R} \setminus \{0\}$. Lemma 3 ensures well-posedness of the Stefan–Maxwell equations (15) and (17) supplied with the constraint given in Eq. (14).

3. Transport algorithms

Systems for the transport fluxes and their mathematical properties were given in Section 2. The adequate choice of a numerical method to solve these systems is now discussed.

In the absence of rounding errors, the solution of a non-singular system using a direct method is exact and requires a finite and fixed amount of work. The number of operations, dominated by the LU decomposition step, scales as $n^3/3$ for large values of the system size n. An operation is defined as one addition plus one multiplication. Rounding errors can be handled by pivoting strategies. For symmetric positive definite matrices, the number of operations is halved to $n^3/6$ using an LDL^{T} decomposition. Furthermore, no pivoting is required.

Krylov projection iterative methods are widely used to solve large sparse linear systems such as those obtained in the discretization of partial differential equations. Ern and Giovangigli [21] have applied a Krylov method to dense linear systems yielding the transport fluxes of neutral mixtures. The conjugate gradient (CG) method for symmetric positive definite matrices appears to be a natural choice, since it combines both properties of residual minimization and simple recurrence formula. Moreover, iterative methods are generally used in combination with some preconditioner accelerating convergence of the method. The CG is associated with a diagonal preconditioner to obtain the transport properties of partially ionized plasmas. For large dense systems of size n, the computational cost of m steps of the CG is of the order of mn^2 operations. For a singular system, the CG method does not fail, contrary to a direct method. Therefore, it is possible to apply the CG algorithm to a symmetric positive semi-definite constrained system and then project the solution on the constraint subspace. The preconditioner matrix must be symmetric positive definite.

3.1. Shear stress and heavy particle heat flux

In the system $G^{\mu}\alpha^{\mu} = \beta^{\mu}$ for the heavy particle shear viscosity $\mu = \eta$ or translational thermal conductivity $\mu = \lambda_{\mathrm{h}}$, the matrix $G^{\mu} \in \mathbb{R}^{N-1,N-1}$ is symmetric positive definite (see Proposition 1). The system can be

solved by means of the LDL^{T} decomposition in $N^3/6$ operations. On the other hand, m steps of the CG method yield an approximate solution in mN^2 operations. The CG preserves positive transport coefficients, even if the iterative procedure is stopped before convergence. The iterative method is computationally less expensive than the direct method provided that the inequality $m < N/6$ is satisfied.

3.2. Diffusion velocities

The matrix $G^{\mathbf{V}}$ is symmetric positive semi-definite and its nullspace reads $\mathscr{R}^{\mathbf{V}}$ (see Proposition 5). Lemma 3 allows for this matrix to be replaced by its non-singular form $G^{\mathbf{V}} + a\mathscr{G}^{\mathbf{V}} \otimes \mathscr{G}^{\mathbf{V}}$ in Eq. (15). Quantity a is adequately chosen such that $\mathrm{O}(G^{\mathbf{V}}) = \mathrm{O}(\mathscr{G}^{\mathbf{V}})$, for instance $a = 1/\max(\mathscr{D}_{ij})$. Provided that the electric field is known a priori, the non-singular system can be solved using the LDL^{T} decomposition. Alternatively, the CG method for constrained system can be applied to the singular form, with the projector $P^{\mathbf{V}}_{ij} = \delta_{ij} - \mathscr{R}^{\mathbf{V}}_i \mathscr{G}^{\mathbf{V}}_j / [(\mathscr{R}^{\mathbf{V}})^{\mathrm{T}} \mathscr{G}^{\mathbf{V}}]$, $i, j \in \mathscr{S}$. In this work, the Stefan–Maxwell equation is preferred to the transport systems for the diffusion coefficients D_{ij}. Indeed, iterative conjugate gradient solutions of these systems do not generally provide symmetric diffusion coefficients until convergence is achieved [22].

When the electric field is ambipolar, the generalized Stefan–Maxwell Eq. (15) is supplied with Eq. (21). The electric field is determined together with the diffusion velocities from the system

$$\begin{pmatrix} G^{\mathbf{V}} & -\kappa^{\Theta}/s \\ -\kappa^{\mathrm{T}}/s & 0 \end{pmatrix} \begin{pmatrix} \mathbf{V} \\ s\mathbf{E} \end{pmatrix} = \begin{pmatrix} -\mathbf{d}^{\Theta\prime} \\ 0 \end{pmatrix}, \tag{23}$$

where $\kappa^{\Theta}_i = \kappa_i \Theta_i$, $\mathbf{d}^{\Theta\prime}_i = \mathbf{d}'_i \Theta_i$, $\Theta_i = T_{\mathrm{h}}/T_i$, $i \in \mathscr{S}$. Quantity $s = \|\kappa\|$ is a scaling factor. The system is supplied with the mass conservation constraint [see Eq. (14)]. As usual, a submatrix $G^{\mathbf{V}} + a\mathscr{G}^{\mathbf{V}} \otimes \mathscr{G}^{\mathbf{V}}$ allows for a non-singular form of the system given by Eq. (23) to be introduced. Both singular and non-singular systems are indefinite and non-symmetric. The non-singular form can be solved by a direct Gaussian elimination with possible pivoting, whereas a Krylov projection iterative method such as the GMRES [23] is suitable for the singular form, associated with the projector $P^{\mathbf{V}}_{ij}$, $i, j \in \mathscr{S}$, for the diffusion velocities onto the constraint subspace along the nullspace of $G^{\mathbf{V}}$. In thermal equilibrium ($T_{\mathrm{h}} = T_{\mathrm{e}}$, $\kappa^{\Theta} = \kappa$), the system becomes symmetric but indefinite. A symmetric Gaussian elimination is retained as direct method. Concerning a Krylov projection iterative method, the GMRES is still applicable in thermal equilibrium but the symmetry property allows for the MINRES [24] to be used instead. The solution of Eq. (17) can be obtained by similar methods, substituting matrix $\tilde{G}^{\mathbf{V}}$ to matrix $G^{\mathbf{V}}$. Eq. (18) is valid for an ambipolar field. In this case, the electric field is readily given by $\mathbf{E} = \mathbf{d}'_{\mathrm{e}}/\kappa_{\mathrm{e}}$. The non-singular matrix $\hat{G}^{\mathbf{V}} + a\hat{\mathscr{G}}^{\mathbf{V}} \otimes \hat{\mathscr{G}}^{\mathbf{V}}$ allows for the LDL^{T} decomposition to be used, whereas the projector $\hat{P}^{\mathbf{V}}_{ij} = \delta_{ij} - \hat{\mathscr{R}}^{\mathbf{V}}_i \hat{\mathscr{G}}^{\mathbf{V}}_j / [(\hat{\mathscr{R}}^{\mathbf{V}})^{\mathrm{T}} \hat{\mathscr{G}}^{\mathbf{V}}]$, $i, j \in \mathscr{H}$, is associated with the CG method. Finally, for vanishing mole fraction of charged species, expression s tends to zero. In Section 4, the electric field is shown to grow unboundly for the particular case of a neutral mixture in local thermodynamic equilibrium, when charged species disappear ($\lim_{s\to 0^+} \mathbf{E} = +\infty$, whereas $\lim_{s\to 0^+} s\mathbf{E} = 0$).

4. Results

The transport algorithms for partially ionized and unmagnetized plasmas introduced in Section 3 have been implemented in the *MUTATION* library. An 11-species air plasma in local thermodynamic equilibrium (LTE) allows for the various numerical methods to be assessed ($T_{\mathrm{h}} = T_{\mathrm{e}} = T$). The mixture chemical components read: N_2, NO, O_2, N, O, N_2^+, NO^+, O_2^+, N^+, O^+, and e^-. Evaluation of the composition is based upon conservation of elements O and N, and charge in the mixture. The mixture is composed of 79% of nitrogen and 21% of oxygen. The net charge is zero. Equilibrium conditions of independent chemical

reactions complete the set of equations. The Newton iterative procedure of Bottin et al. [25] yields mole fractions. The collision integrals set employed is described in [25]. The conditions on the collision integrals $B^*_{ij} < 25/12,\ 5\bar{Q}^{(1,2)}_{ie} - 4\bar{Q}^{(1,3)}_{ie} < 25\bar{Q}^{(1,1)}_{ie}/12,\ i,j \in \mathscr{H},\ i \neq j$, and $\varphi_{ij} > -1,\ i,j \in \mathscr{S},\ i \neq j$, formulated in Propositions 1,2 and 4,5,6 have been verified to hold for all thermodynamic states considered. Pressure is kept constant at 1 atm and temperature varies between 250 and 15 000 K. First, the physical model is evaluated comparing results obtained with the direct methods to literature data. Eventually, the iterative methods are confronted with mixture rules with respect to accuracy and computational cost, the direct methods being employed as reference in term of accuracy.

4.1. Physical model

4.1.1. Shear viscosity

The shear viscosity computed by means of Eq. (3) is displayed in Fig. 1. Below the ionization range, it increases with temperature and presents some modulations linked to changes of composition due to molecular dissociation. Above 10,000 K, large ion-ion cross-sections drastically decrease the shear viscosity.

4.1.2. Heat and mass fluxes

In order to provide some pragmatic treatment of the internal degrees of freedom, a passive transport of the internal energy is considered, neglecting inelastic collisions. The species enthalpy of heavy particles given in Eq. (5) is modified accordingly

$$h_i = h_{Ti} + h_{Ei} + h_{Fi}, \quad i \in \mathscr{H}_a, \tag{24a}$$

$$h_i = h_{Ti} + h_{Ri} + h_{Vi} + h_{Ei} + h_{Fi}, \quad i \in \mathscr{H}_p, \tag{24b}$$

where $\mathscr{H}_a$ and $\mathscr{H}_p$ stand for the set of indices of atoms and polyatomic molecules. Expressions h_{Ri}, h_{Vi}, and h_{Ei} correspond to the rotational, vibrational, and electronic species enthalpies. These quantities are evaluated, respectively, at the rotational, vibrational, and electronic temperatures: T_R, T_V, and T_E (in our particular case, $T_R = T_V = T_E = T$). Species enthalpies are derived from a semi-classical statistical

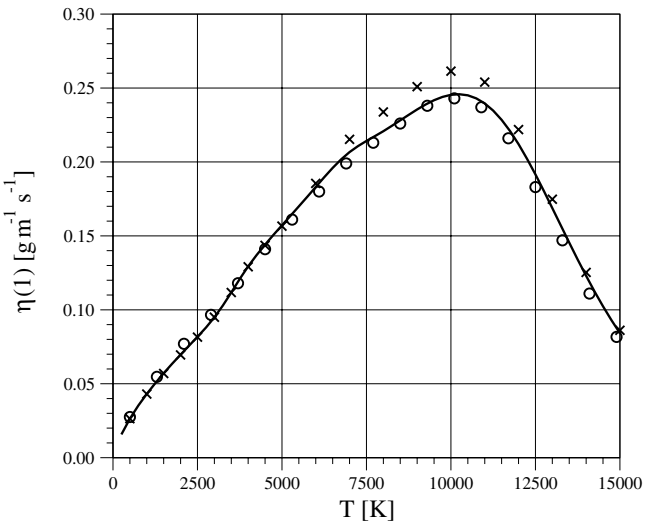

Fig. 1. Shear viscosity of air: –, our results; ×, Capitelli et al. [26], and ○, Murphy [27].

mechanics approach with independent degrees of freedom. Moreover, the heavy particle heat flux is corrected by Eucken's contribution $-\lambda_R \nabla T_R - \lambda_V \nabla T_V - \lambda_E \nabla T_E$. Rotational, vibrational, and electronic thermal conductivities are given by

$$\lambda_R = n \sum_{i \in \mathscr{H}_p} \frac{x_i C_i^R}{\sum_{j \in \mathscr{H}} x_j / \mathscr{D}_{ij}}, \tag{25a}$$

$$\lambda_V = n \sum_{i \in \mathscr{H}_p} \frac{x_i C_i^V}{\sum_{j \in \mathscr{H}} x_j / \mathscr{D}_{ij}}, \tag{25b}$$

$$\lambda_E = n \sum_{i \in \mathscr{H}} \frac{x_i C_i^E}{\sum_{j \in \mathscr{H}} x_j / \mathscr{D}_{ij}}, \tag{25c}$$

where C_i^R, C_i^V, and C_i^E are the rotational, vibrational, and electronic species specific heats per particle. Binary diffusion coefficients $\mathscr{D}_{ij}$ are defined in Appendix A.

The heat flux components per temperature gradient are compared in Fig. 2. The diffusion heat flux $\sum_{j \in \mathscr{S}} \rho_j h_j \mathbf{V}_j$ yields the dominant contribution for temperature ranges 2500–9000 and 11,000–15,000 K. The peaks correspond to the dissociation peaks of O_2 and N_2 and the ionization peak of nitrogen and oxygen atoms. Diffusion velocities are deduced from Eq. (15) in the second Laguerre–Sonine approximation. An electric field, gradients of pressure, temperature, and concentration generate mass fluxes. We envisage the effect of a thermal gradient on the diffusion velocities, in relation with variations of the equilibrium composition and ambipolar electric field. The influence of an external electric field or pressure gradient is not considered. Therefore, the driving forces read $\mathbf{d}_i = (\partial x_i / \partial T) \nabla T - \kappa_i \mathbf{E}$, where $\mathbf{E}$ is the ambipolar field. The electron thermal conductivity λ_e given in Eq. (10) becomes significant beyond 7000 K. The second Laguerre–Sonine approximation underestimates the magnitude of λ_e, a third-order approximation is required. The heavy particle thermal conductivity $\lambda_h(2)$ and internal thermal conductivity $\lambda_R + \lambda_V + \lambda_E$ are

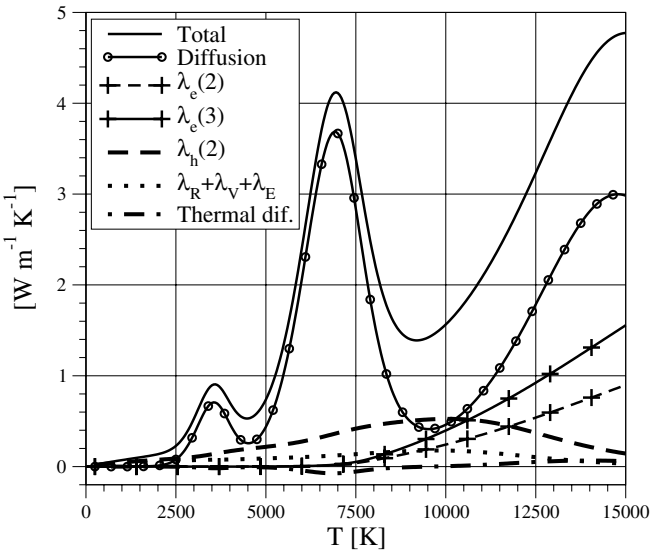

Fig. 2. Heat flux components of air, per temperature gradient.

computed using Eqs. (6) and (25). Their influence is major below 2500 K and between the peaks of diffusion heat flux. The thermal diffusion heat flux $p\sum_{j\in\mathscr{S}}[k^{\mathrm{h}}_{\mathrm{T}j}(2)+k^{\mathrm{e}}_{\mathrm{T}j}(3)]\mathbf{V}_j$ weakly contributes to the total heat flux in LTE plasmas.

Major heavy particle thermal diffusion ratios $k^{\mathrm{h}}_{\mathrm{T}j}(2)$ computed using Eq. (7) are shown in Fig. 3, whereas major electron thermal diffusion ratios $k^{\mathrm{e}}_{\mathrm{T}j}$ deduced from Eq. (11) are presented in Fig. 4. The Laguerre–Sonine approximation order is referred to symbol ξ. The third Laguerre–Sonine approximation is necessary to accurately compute $k^{\mathrm{e}}_{\mathrm{T}j}$.

The variants of the Stefan–Maxwell equations (15), (17), and (18) are, respectively, denoted by SM1, SM2, and SM3. The diffusion heat flux computed by means of Eq. (15) with a second-order Laguerre–Sonine approximation (i.e., SM1 with $\xi=2$) serves as reference. Heavy particle thermal diffusion is evaluated with $\xi=2$, whereas electron thermal diffusion is computed with $\xi=3$. As demonstrated in Fig. 5, both approximations SM2 and SM3 with $\xi=2$ are accurate, the relative error on the diffusion heat flux being inferior to 10^{-3}. Results are also obtained using SM1 with $\xi=1$ and no thermal diffusion. The major error is caused by the absence of thermal diffusion (more than 10% around 5000 K and 4% above 12,000 K). This is verified by using SM1 still with $\xi=1$ but including thermal diffusion (maximum 3% of error). Butler and Brokaw [28] have derived a formula for a reactive thermal conductivity to compute the diffusion heat flux of a mixture in LTE. This formula remains valid in ionized mixtures with an ambipolar field [25], but does not incorporate pressure and thermal diffusion. Moreover, Butler and Brokaw's formula does not account for elemental demixing. This formula generates more than 25% of relative error about 4000 K and above 14,000 K.

The ambipolar electric field is displayed in Fig. 6. It is eliminated from SM3 and reads $\mathbf{E}=\mathbf{d}'_{\mathrm{e}}/\kappa_{\mathrm{e}}$. The electron mole fraction tends to zero faster than the electron driving force when temperature decreases below 2500 K. Consequently, the ambipolar electric field grows unboundly when temperature decreases under this threshold. The ambipolar electric field is still present in SM1 and SM2. Nevertheless, the method to solve these equations remains robust since the term $\kappa_i\mathbf{E},\ i\in\mathscr{S}$, cancels out at low temperature.

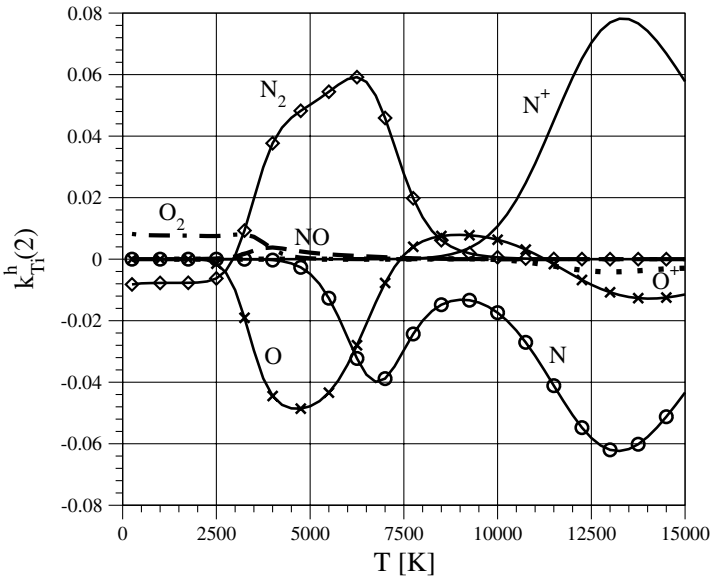

Fig. 3. Major heavy particle thermal diffusion ratios of air.

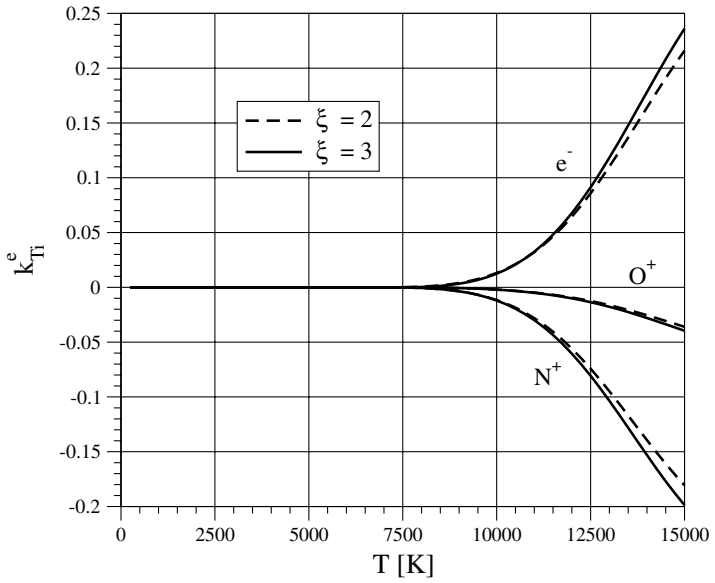

Fig. 4. Major electron thermal diffusion ratios of air: —, $k^e_{Tj}(2)$ and --- $k^e_{Tj}(3)$.

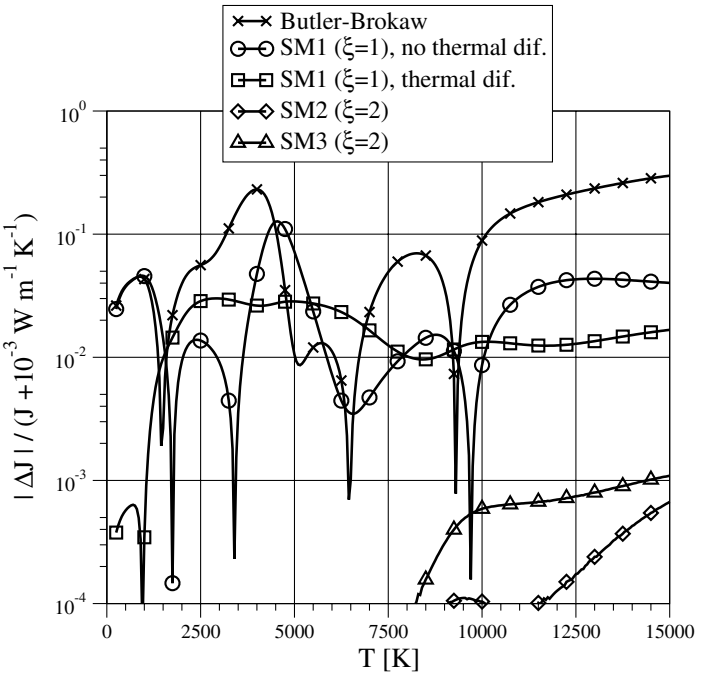

Fig. 5. Relative error on diffusion heat flux computed using different forms of the Stefan–Maxwell equation and Butler and Brokaw's formula [28].

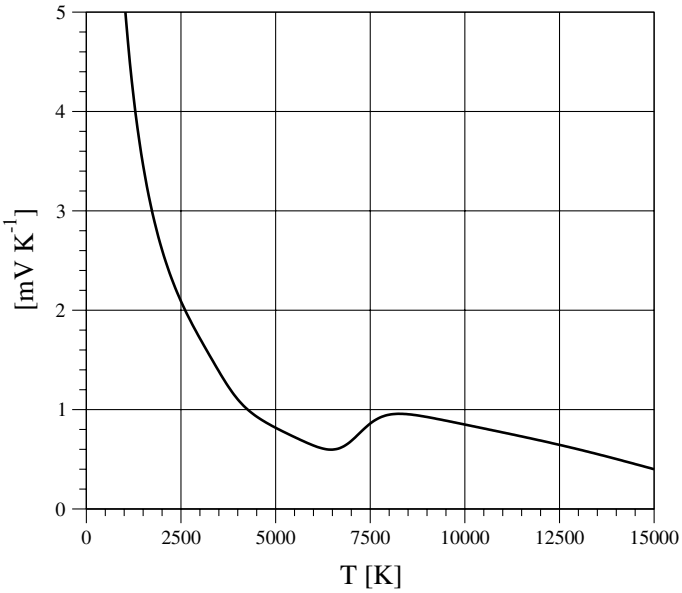

Fig. 6. Ambipolar electric field of air, per temperature gradient.

The total heat flux is compared in Fig. 7 to the computed results of Capitelli et al. [26] and Murphy [27], and experimental values of Azinovsky et al. [29]. Two different physical situations are depicted. First, the driving forces are due to concentration gradients induced by a thermal gradient in an equilibrium mixture with frozen elemental fractions including thermal diffusion, the Stefan–Maxwell equation supplies with the diffusion velocities. Second, no possible diffusion of elements is allowed, the diffusion heat flux is computed

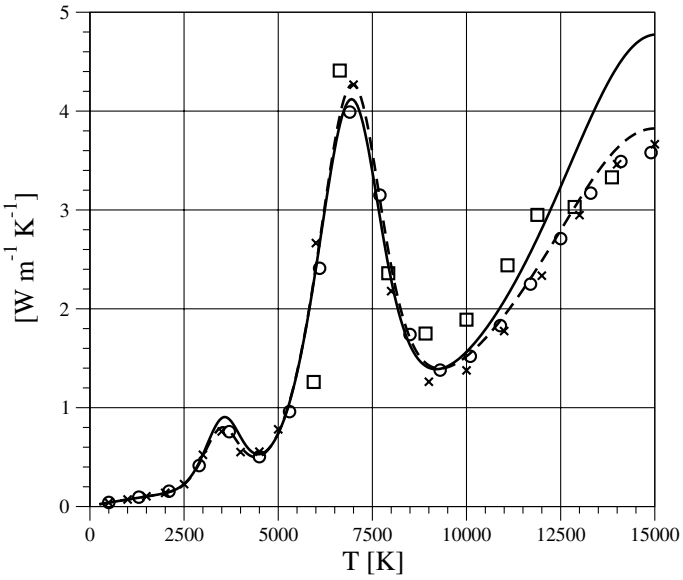

Fig. 7. Total heat flux of air per temperature gradient: —, Stefan–Maxwell, our results; - - - Butler–Brokaw, our results; ×, Capitelli et al. [26]; ○, Murphy [27], and □, Azinovsky et al. [29].

by means of the Butler–Brokaw formula. Capitelli et al. [26] and Murphy [27] have used the Butler–Brokaw formula.

4.1.3. Electrical conductivity

We consider now a plasma influenced by an electric field and without any spatial gradients. It is established in Section 2.2 that the electrical conductivity does not depend on ions. This can be verified by using Eq. (15) without any spatial gradients and a unit electric field. The conduction current corresponds then to the electrical conductivity. The electrical conductivity σ_e calculated in a simpler manner from Eq. (20) is compared in Fig. 8 to the computed results of Capitelli et al. [26] and Murphy [27], and experimental values of Azinovsky et al. [29]. The second Laguerre–Sonine approximation yields accurate results.

4.2. Computational aspects

Approximate formulas and rules to compute mixture transport properties abound in the literature [12,13]. Wilke's rule [7] and Gupta–Yos's formulas [8] are widely used in the computational fluid dynamics field to estimate the heavy particle shear viscosity and translational thermal conductivity. Sutton and Gnoffo [30] have also developed an algorithm to solve the Stefan–Maxwell equation. The accuracy and computational efficiency of these mixture rules, the Sutton–Gnoffo algorithm, and our methods are evaluated. The computational time corresponds to one million of calls to the tested routine for sixty temperature points from 250 to 15,000 K. The number of iterations of the various iterative methods is selected empirically based on the residual norm, such that the relative error on the transport property remains below 1%.

4.2.1. Shear viscosity

The relative error on the shear viscosity is presented in Fig. 9. Wilke's rule leads to a relative error about 10% in the dissociation range rising up to 70% in the ionization range. Below 9000 K, the Gupta–Yos formula is accurate and one CG iteration is sufficiently precise. Above this temperature threshold, the

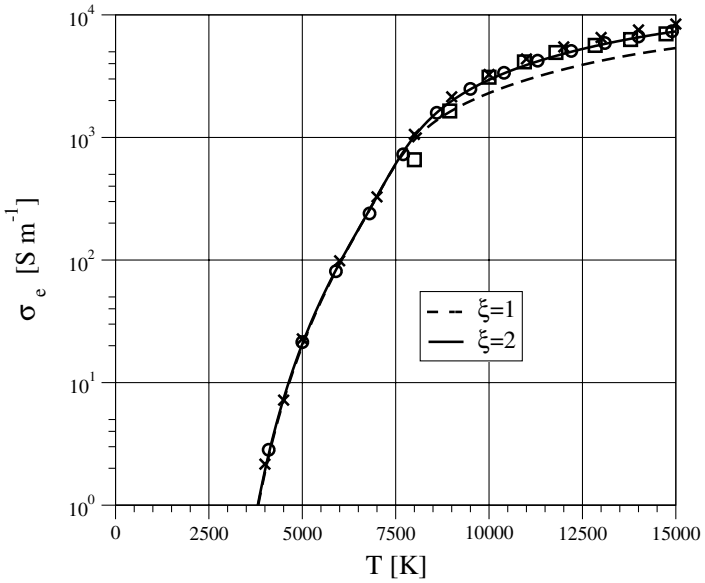

Fig. 8. Electrical conductivity of air: ---, $\sigma_e(1)$, our results; —, $\sigma_e(2)$, our results; ×, Capitelli et al. [26]; ○, Murphy [27]; and □, Azinovsky et al. [29].

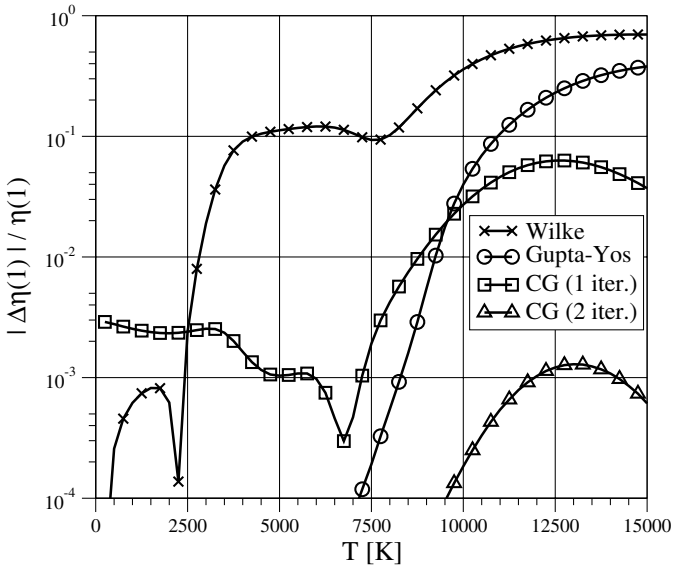

Fig. 9. Relative error on shear viscosity of air.

Table 1
Computational cost of η

CG	1.00
Direct	1.51
Gupta–Yos	1.03
Wilke	2.16

Gupta–Yos formula fails with a maximum relative error of 40%, whereas one CG iteration yields maximum 6% of error. Two CG iterations provide accurate results.

The computational cost is summarized in Table 1. Wilke's rule for the shear viscosity requires $3N - 3$ square roots to be evaluated. The number of operations of the Gupta–Yos formula scales as $N^2/2$. The CG is the cheapest and most accurate method.

4.2.2. Heavy particle translational thermal conductivity

Fig. 10 reveals that similar conclusions hold for accuracy of the different methods to evaluate the heavy particle translational thermal conductivity. The computational cost is shown in Table 2. The Gupta–Yos formula for the thermal conductivity requires N^2 operations and is more expensive than the formula for the shear viscosity. The CG remains the cheapest method.

4.2.3. Heavy particle thermal diffusion ratios

The relative error on the thermal diffusion heat flux is presented in Fig. 11. Diffusion velocities are calculated with a direct method. Three CG iterations are sufficient to estimate with accuracy the heavy particle thermal diffusion ratios.

Thermal diffusion ratios computed together with the translational thermal conductivity necessitate one matrix vector product, i.e., N^2 operations. This explains the computational cost given in Table 3.

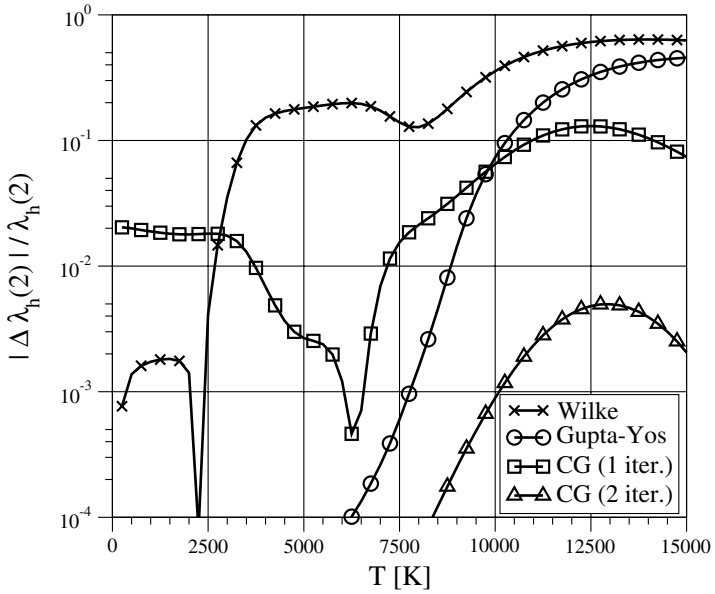

Fig. 10. Relative error on heavy particle translational thermal conductivity.

Table 2
Computational cost of λ_h

CG	1.00
Direct	1.59
Gupta–Yos	2.18
Wilke	2.31

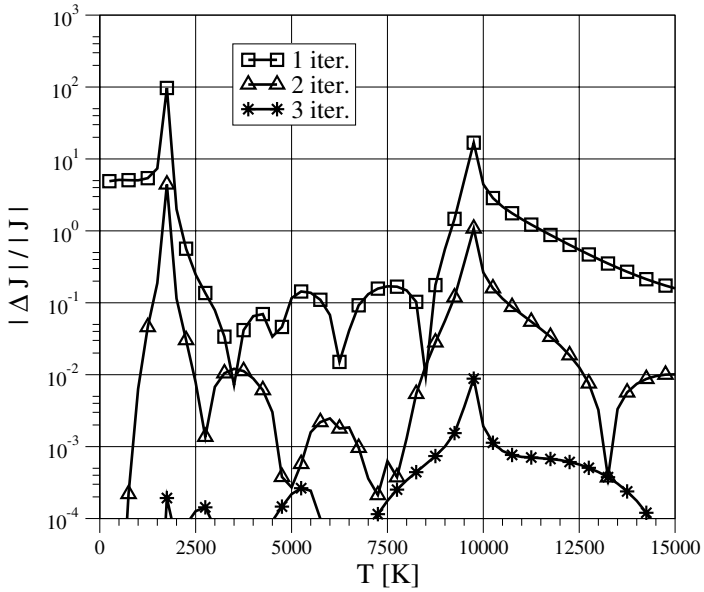

Fig. 11. Relative error on heavy particle thermal diffusion heat flux using the CG.

Table 3
Computational cost of $k^{h}_{Ti},\ i \in \mathscr{H}$

	λ_h and k^{h}_{Ti}	λ_h
CG	1.00	0.47
Direct	1.18	0.76

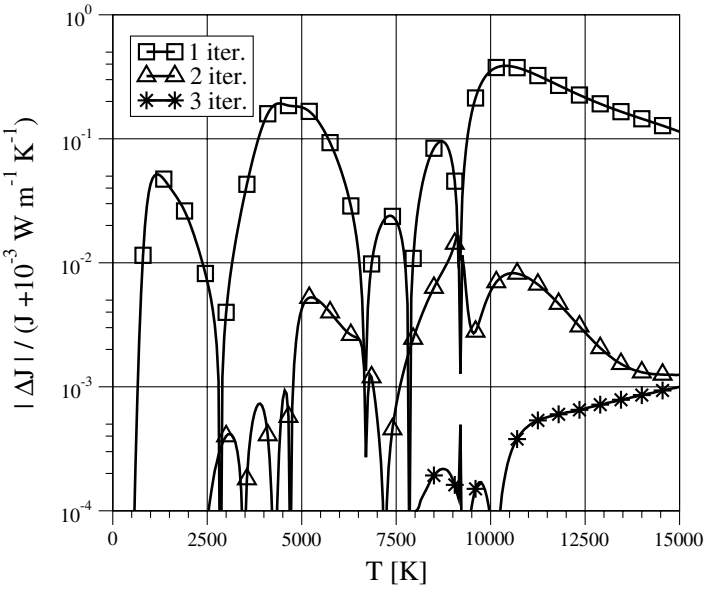

Fig. 12. Relative error on diffusion heat flux using the CG (SM3).

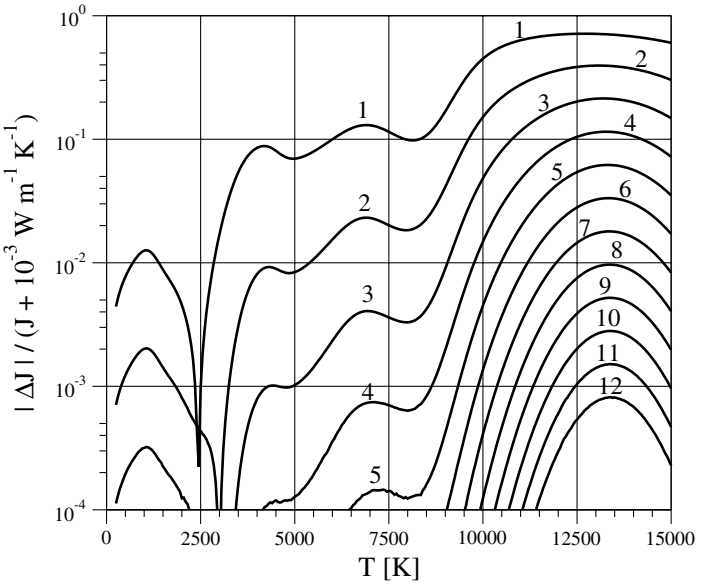

Fig. 13. Relative error on diffusion heat flux using the Sutton–Gnoffo algorithm (SM3).

4.2.4. Stefan–Maxwell equation

Three iterative methods are tested to obtain the diffusion velocities. Two CG iterations are necessary to accurately solve for SM3 (see Fig. 12). The Sutton–Gnoffo algorithm applied to the same equation presents a slower convergence as shown in Fig. 13. The GMRES applied to SM1 requires four iterations for a converged result (see Fig. 14).

Table 4 establishes that the CG applied to SM3 remains the fastest method.

4.2.5. Computational cost

The absolute and relative computational cost of the transport properties is summarized in Table 5. Evaluation of the electron properties $\lambda_e(3)$, $k^e_{Ti}(3),\ i \in \mathscr{S}$, $\sigma_e(2)$, and $\varphi_{ie}(2),\ i \in \mathscr{H}$, corresponds to about 1% of the total cost. Therefore, these quantities are not displayed in the table. Second-order corrections of the Stefan–Maxwell equation are expensive. The evaluation of the transport collision integrals is more expensive than a typical transport property computation.

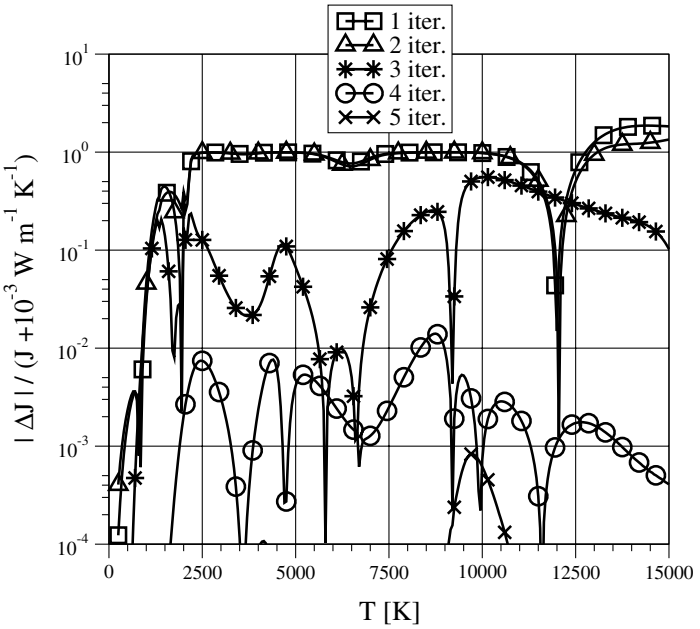

Fig. 14. Relative error on diffusion heat flux using the GMRES (SM1).

Table 4
Computational cost of $\mathbf{V}_i,\ i \in \mathscr{S}$

CG (SM3)	1.00
Direct (SM3)	1.90
Sutton–Gnoffo (SM3)	2.70
GMRES (SM1)	2.66
Direct (SM1)	3.03

Table 5
Computational cost, summary

	Absolute (s)	Relative (%)
$\varphi_{ij}(2),\ i,j \in \mathscr{H},\ i \neq j$	4809	36.9
Collision integrals	4410	33.9
$\lambda_{\mathrm{h}}(2)$ and $k^{\mathrm{h}}_{\mathrm{T}i}(2),\ i \in \mathscr{H}$ (CG)	1664	12.8
$\eta(1)$ (CG)	838	6.4
$\mathbf{V}_i,\ i \in \mathscr{S}$ (CG, SM3)	824	6.3
$\lambda_{\mathrm{R}} + \lambda_{\mathrm{V}} + \lambda_{\mathrm{E}}$,	301	2.3
Total	13,030	100.0

5. Conclusions

The new formalism for the transport properties of partially ionized and unmagnetized plasmas derived in [1] was envisaged under a computational perspective. We established well-posedness of the transport property expressions, provided that some conditions on the kinetic data are met. The mathematical structure of the transport matrices was readily used to build transport algorithms inspired by Ern and Giovangigli [21]. The LDL^{T} decomposition was chosen as direct solver. Various convergent iterative Krylov projection methods were also presented. The constrained Stefan–Maxwell equation required a special treatment for mass conservation. A non-singular yet symmetric form was introduced in the case of direct methods and a suitable projector was associated with iterative methods.

Validity of the physical model and efficiency of the algorithms were examined for an 11-species air plasma in LTE. We recommend one non-vanishing Laguerre–Sonine contribution to evaluate the shear stress and heat and mass fluxes of heavy particle properties, whereas two non-vanishing Laguerre–Sonine contributions are requested for electron properties. Concerning the heavy-particle shear viscosity and thermal conductivity, mixture rules of Wilke and Gupta–Yos were shown to be less accurate and generally more expensive than the CG with a diagonal preconditioner. Therefore, these mixture rules must be abandoned in favor of the CG. In the case of ambipolar diffusion, an approximation of the Stefan–Maxwell equation involving only heavy particle velocities is retained. In that model, the ambipolar field is proportional to the electron driving force. The CG with a diagonal preconditioner and a projection step to ensure mass conservation constitutes the most efficient method to obtain the diffusion velocities.

The transport algorithms can be further applied to computational fluid dynamics simulations in LTE or in thermo-chemical non-equilibrium. A suitable flow simulation will allow for concentration, pressure, and temperature gradients effects on diffusion fluxes to be analyzed. Finally, for mixtures composed of a large number of species, superiority of the iterative methods with respect to the direct methods will be indisputable.

Acknowledgements

We gratefully acknowledge Alexandre Ern from the École Nationale des Ponts et Chaussées, Marne La Vallée, and Vincent Giovangigli from the École Polytechnique, Palaiseau, for providing the sources of their *EGLIB* library for the multicomponent transport properties of mixtures composed of neutral species. Many computational issues of *MUTATION* were inspired from *EGLIB*. This work is supported in part by a contract from the European Space Agency, D. Giordano Technical Monitor.

Appendix A. Collision integrals

The deflection angle χ is related to the interaction potential $\varphi(r)$

$$\chi = \pi - 2b \int_{r_m}^{\infty} \frac{\mathrm{d}r/r^2}{\sqrt{1 - b^2/r^2 - \varphi(r)/\left(\frac{1}{2}\frac{m_i m_j}{m_i+m_j} g^2\right)}}, \tag{A.1}$$

where b is the impact parameter, r the distance between colliding particles, r_m the distance of closest approach, m_i the mass of species i, and g the relative velocity of colliding particles. Cross-sections are given in terms of the deflection angle

$$Q_{ij}^{(l)} = 2\pi \int_0^{\infty} \left(1 - \cos^l \chi\right) b \, \mathrm{d}b. \tag{A.2}$$

Reduced collision integrals $\bar{Q}_{ij}^{(l,s)}$ and binary diffusion coefficients $\mathscr{D}_{ij}$ are presented in thermal non-equilibrium, in relation with the dimensional collision integrals $\Omega_{ij}^{(l,s)}$ defined in [1]. Introducing a reference length σ_{ij} of the interaction potential, reduced collision integrals $\Omega_{ij}^{(l,s)^*}$ in the nomenclature of Hirschfelder et al. [6] or Ferziger and Kaper [5] are also explicited to avoid any ambiguity. The collision integrals and binary diffusion coefficients are symmetric in the species.

- Heavy–heavy interactions, $i, j \in \mathscr{H}$.

$$\begin{aligned} \bar{Q}_{ij}^{(l,s)} &= \pi \sigma_{ij}^2 \Omega_{ij}^{(l,s)^*} = \sqrt{\frac{2\pi}{k_\mathrm{B} T_\mathrm{h}} \frac{m_i m_j}{m_i + m_j}} \frac{4(l+1)}{(s+1)!\left[2l + 1 - (-1)^l\right]} \Omega_{ij}^{(l,s)} \\ &= \frac{4(l+1)}{(s+1)!\left[2l + 1 - (-1)^l\right]} \int_0^{\infty} \exp\left(-\gamma^2\right) \gamma^{2s+3} Q_{ij}^{(l)} \, \mathrm{d}\gamma, \end{aligned} \tag{A.3a}$$

$$n\mathscr{D}_{ij} = \sqrt{\frac{2\pi k_\mathrm{B} T_\mathrm{h}\left(m_i + m_j\right)}{m_i m_j}} \frac{3}{16 \bar{Q}_{ij}^{(1,1)}}, \tag{A.3b}$$

where $\gamma = \{m_i m_j/[(m_i + m_j) 2 k_\mathrm{B} T_\mathrm{h}]\}^{1/2} g$. Usual combinations of collision integrals are introduced

$$A_{ij}^* = \frac{\bar{Q}_{ij}^{(2,2)}}{\bar{Q}_{ij}^{(1,1)}}, \tag{A.4a}$$

$$B_{ij}^* = \frac{5\bar{Q}_{ij}^{(1,2)} - 4\bar{Q}_{ij}^{(1,3)}}{\bar{Q}_{ij}^{(1,1)}}, \tag{A.4b}$$

$$C_{ij}^* = \frac{\bar{Q}_{ij}^{(1,2)}}{\bar{Q}_{ij}^{(1,1)}}. \tag{A.4c}$$

Shear viscosity coefficients read

$$\eta_i = \frac{5}{16} \frac{\sqrt{\pi k_\mathrm{B} T_\mathrm{h} m_i}}{\bar{Q}_{ii}^{(2,2)}}. \tag{A.5}$$

- Heavy–electron interactions, $i \in \mathscr{H}$

$$\bar{Q}_{ie}^{(l,s)} = \pi\sigma_{ie}^2 \Omega_{ie}^{(l,s)^*} = \sqrt{\frac{2\pi m_e}{k_B T_e}} \frac{4(l+1)}{(s+1)!\left[2l+1-(-1)^l\right]} \Omega_{ie}^{(l,s)}$$
$$= \frac{4(l+1)}{(s+1)!\left[2l+1-(-1)^l\right]} \int_0^\infty \exp\left(-g^2\right) g^{2s+3} Q_{ie}^{(l)} \, \mathrm{d}g, \tag{A.6a}$$

$$n\mathscr{D}_{ie} = \sqrt{\frac{2\pi k_B T_e}{m_e}} \frac{3}{16 \bar{Q}_{ie}^{(1,1)}}, \tag{A.6b}$$

where $g = [m_e/(2k_B T_e)]^{1/2} g$.

- Electron–electron interactions

$$\bar{Q}_{ee}^{(l,s)} = \pi\sigma_{ee}^2 \Omega_{ee}^{(l,s)^*} = \sqrt{\frac{\pi m_e}{k_B T_e}} \frac{4(l+1)}{(s+1)!\left[2l+1-(-1)^l\right]} \Omega_{ee}^{(l,s)}$$
$$= \frac{4(l+1)}{(s+1)!\left[2l+1-(-1)^l\right]} \int_0^\infty \exp\left(-g^2\right) g^{2s+3} Q_{ee}^{(l)} \, \mathrm{d}g, \tag{A.7a}$$

$$n\mathscr{D}_{ee} = \sqrt{\frac{\pi k_B T_e}{m_e}} \frac{3}{8 \bar{Q}_{ee}^{(1,1)}}, \tag{A.7b}$$

where $g = [m_e/(4k_B T_e)]^{1/2} g$.

Appendix B. Elastic energy exchange

The energy exchanged by elastic collisions between electrons and heavy particles reads

$$\Delta E_e^0 = \frac{\frac{3}{2} n_e k_B (T_h - T_e)}{\tau}, \tag{B.1}$$

where the relaxation time τ is given by

$$\frac{1}{\tau} = \frac{8}{3} \sum_{j \in \mathscr{H}} \frac{m_e}{m_j} \sqrt{\frac{8 k_B T_e}{\pi m_e}} n_j \bar{Q}_{ej}^{(1,1)}. \tag{B.2}$$

Appendix C. Transport systems

- Heavy particle subsystem, $i, j \in \mathscr{H}$

$$G_{ij}^{\eta} = G_{ji}^{\eta} = \frac{1}{T_h} H_{ij}^{00} = \frac{x_i x_j}{n\mathscr{D}_{ij}} \frac{1}{(m_i + m_j)} \left(\frac{6}{5} A_{ij}^* - 2 \right), \quad i \neq j, \tag{C.1a}$$

$$G_{ii}^{\eta} = \frac{1}{T_{\mathrm{h}}} H_{ii}^{00} = \sum_{\substack{j\in\mathscr{H}\\ j\neq i}} \frac{x_i x_j}{n\mathscr{D}_{ij}} \frac{1}{(m_i+m_j)} \left(\frac{6}{5}\frac{m_j}{m_i} A_{ij}^{*} + 2 \right) + \frac{x_i^2}{\eta_i}, \tag{C.1b}$$

$$G_{ij}^{\lambda_{\mathrm{h}}} = G_{ji}^{\lambda_{\mathrm{h}}} = \Lambda_{ij}^{11} = \frac{1}{25k_{\mathrm{B}}} \frac{x_i x_j}{n\mathscr{D}_{ij}} \frac{m_i m_j}{(m_i+m_j)^2} \left(16A_{ij}^{*} + 12B_{ij}^{*} - 55 \right), \quad i \neq j, \tag{C.1c}$$

$$G_{ii}^{\lambda_{\mathrm{h}}} = \Lambda_{ii}^{11} = \frac{1}{25k_{\mathrm{B}}} \sum_{\substack{j\in\mathscr{H}\\ j\neq i}} \frac{x_i x_j}{n\mathscr{D}_{ij}} \frac{1}{(m_i+m_j)^2} \left(30m_i^2 + 25m_j^2 - 12m_j^2 B_{ij}^{*} + 16 m_i m_j A_{ij}^{*} \right) + \frac{4}{15k_{\mathrm{B}}} \frac{x_i^2 m_i}{\eta_i}, \tag{C.1d}$$

$$\Lambda_{ij}^{01} = \Lambda_{ji}^{10} = \frac{1}{25k_{\mathrm{B}}} \frac{x_i x_j}{n\mathscr{D}_{ij}} \frac{m_i}{(m_i+m_j)} \left(12C_{ij}^{*} - 10 \right), \quad i \neq j, \tag{C.1e}$$

$$\Lambda_{ii}^{01} = \Lambda_{ii}^{10} = -\frac{1}{25k_{\mathrm{B}}} \sum_{\substack{j\in\mathscr{H}\\ j\neq i}} \frac{x_i x_j}{n\mathscr{D}_{ij}} \frac{m_j}{(m_i+m_j)} \left(12C_{ij}^{*} - 10 \right), \tag{C.1f}$$

$$G_{ij}^{\mathbf{V}} = G_{ji}^{\mathbf{V}} = \tilde{G}_{ij}^{\mathbf{V}} = \tilde{G}_{ji}^{\mathbf{V}} = \hat{G}_{ij}^{\mathbf{V}} = \hat{G}_{ji}^{\mathbf{V}} = -\frac{x_i x_j}{\mathscr{D}_{ij}} (1+\varphi_{ij}), \quad i \neq j, \tag{C.1g}$$

$$G_{ii}^{\mathbf{V}} = \sum_{\substack{j\in\mathscr{H}\\ j\neq i}} \frac{x_i x_j}{\mathscr{D}_{ij}} (1+\varphi_{ij}) + \left(\frac{T_{\mathrm{e}}}{T_{\mathrm{h}}} \right)^2 \frac{x_i x_{\mathrm{e}}}{\mathscr{D}_{i\mathrm{e}}} (1+\varphi_{i\mathrm{e}}), \tag{C.1h}$$

$$\tilde{G}_{ii}^{\mathbf{V}} = \hat{G}_{ii}^{\mathbf{V}} = \sum_{\substack{j\in\mathscr{H}\\ j\neq i}} \frac{x_i x_j}{\mathscr{D}_{ij}} (1+\varphi_{ij}). \tag{C.1i}$$

- Heavy particle-electron subsystem, $i \in \mathscr{H}$

$$\Lambda_{i\mathrm{e}}^{01} = \Lambda_{\mathrm{e}i}^{10} = -\frac{64 x_{\mathrm{e}} x_i}{75k_{\mathrm{B}}} \frac{T_{\mathrm{e}}}{T_{\mathrm{h}}} \sqrt{\frac{m_{\mathrm{e}}}{2\pi k_{\mathrm{B}} T_{\mathrm{e}}}} \left(\frac{5}{2}\bar{Q}_{i\mathrm{e}}^{(1,1)} - 3\bar{Q}_{i\mathrm{e}}^{(1,2)} \right), \tag{C.2a}$$

$$\Lambda_{i\mathrm{e}}^{02} = \Lambda_{\mathrm{e}i}^{20} = -\frac{64 x_{\mathrm{e}} x_i}{75k_{\mathrm{B}}} \frac{T_{\mathrm{e}}}{T_{\mathrm{h}}} \sqrt{\frac{m_{\mathrm{e}}}{2\pi k_{\mathrm{B}} T_{\mathrm{e}}}} \left(\frac{35}{8}\bar{Q}_{i\mathrm{e}}^{(1,1)} - \frac{21}{2}\bar{Q}_{i\mathrm{e}}^{(1,2)} + 6\bar{Q}_{i\mathrm{e}}^{(1,3)} \right), \tag{C.2b}$$

$$G_{i\mathrm{e}}^{\mathbf{V}} = G_{\mathrm{e}i}^{\mathbf{V}} = \tilde{G}_{i\mathrm{e}}^{\mathbf{V}} = -\frac{T_{\mathrm{e}}}{T_{\mathrm{h}}} \frac{x_i x_{\mathrm{e}}}{\mathscr{D}_{i\mathrm{e}}} (1+\varphi_{i\mathrm{e}}), \tag{C.2c}$$

$$\tilde{G}_{\mathrm{e}i}^{\mathbf{V}} = 0. \tag{C.2d}$$

- Electron subsystem

$$\Lambda_{\mathrm{ee}}^{00} = \frac{64 x_{\mathrm{e}}}{75k_{\mathrm{B}}} \sqrt{\frac{m_{\mathrm{e}}}{2\pi k_{\mathrm{B}} T_{\mathrm{e}}}} \sum_{j\in\mathscr{H}} x_j \bar{Q}_{\mathrm{e}j}^{(1,1)}, \tag{C.3a}$$

$$\Lambda_{ee}^{01} = \Lambda_{ee}^{10} = \frac{64x_e}{75k_B}\sqrt{\frac{m_e}{2\pi k_B T_e}}\sum_{j\in\mathscr{H}} x_j\left(\frac{5}{2}\bar{Q}_{ej}^{(1,1)} - 3\bar{Q}_{ej}^{(1,2)}\right), \tag{C.3b}$$

$$\Lambda_{ee}^{11} = \frac{64x_e}{75k_B}\sqrt{\frac{m_e}{2\pi k_B T_e}}\left[\sum_{j\in\mathscr{H}} x_j\left(\frac{25}{4}\bar{Q}_{ej}^{(1,1)} - 15\bar{Q}_{ej}^{(1,2)} + 12\bar{Q}_{ej}^{(1,3)}\right) + x_e\sqrt{2}\bar{Q}_{ee}^{(2,2)}\right], \tag{C.3c}$$

$$\Lambda_{ee}^{02} = \Lambda_{ee}^{20} = \frac{64x_e}{75k_B}\sqrt{\frac{m_e}{2\pi k_B T_e}}\sum_{j\in\mathscr{H}} x_j\left(\frac{35}{8}\bar{Q}_{ej}^{(1,1)} - \frac{21}{2}\bar{Q}_{ej}^{(1,2)} + 6\bar{Q}_{ej}^{(1,3)}\right), \tag{C.3d}$$

$$\begin{aligned}\Lambda_{ee}^{12} = \Lambda_{ee}^{21} = \frac{64x_e}{75k_B}\sqrt{\frac{m_e}{2\pi k_B T_e}}\Bigg[&\sum_{j\in\mathscr{H}} x_j\left(\frac{175}{16}\bar{Q}_{ej}^{(1,1)} - \frac{315}{8}\bar{Q}_{ej}^{(1,2)} + 57\bar{Q}_{ej}^{(1,3)} - 30\bar{Q}_{ej}^{(1,4)}\right)\\ &+ x_e\sqrt{2}\left(\frac{7}{4}\bar{Q}_{ee}^{(2,2)} - 2\bar{Q}_{ee}^{(2,3)}\right)\Bigg],\end{aligned} \tag{C.3e}$$

$$\begin{aligned}\Lambda_{ee}^{22} = \frac{64x_e}{75k_B}\sqrt{\frac{m_e}{2\pi k_B T_e}}\Bigg[&\sum_{j\in\mathscr{H}} x_j\left(\frac{1225}{64}\bar{Q}_{ej}^{(1,1)} - \frac{735}{8}\bar{Q}_{ej}^{(1,2)} + \frac{399}{2}\bar{Q}_{ej}^{(1,3)} - 210\bar{Q}_{ej}^{(1,4)} + 90\bar{Q}_{ej}^{(1,5)}\right)\\ &+ x_e\sqrt{2}\left(\frac{77}{16}\bar{Q}_{ee}^{(2,2)} - 7\bar{Q}_{ee}^{(2,3)} + 5\bar{Q}_{ee}^{(2,4)}\right)\Bigg],\end{aligned} \tag{C.3f}$$

$$G_{ee}^{\mathbf{v}} = \tilde{G}_{ee}^{\mathbf{v}} = \sum_{j\in\mathscr{H}} \frac{x_e x_j}{\mathscr{D}_{ej}}\left(1 + \varphi_{ej}\right). \tag{C.3g}$$

Correction functions are obtained in various Laguerre–Sonine approximations for $\varphi_{ij},\ i,j \in \mathscr{H}$

$$\sum_{k\in\mathscr{H}} G_{ik}^{\lambda_h}\beta_{kj,1}(2) = -2\Lambda_{ji}^{01}, \quad i,j \in \mathscr{H}, \tag{C.4a}$$

$$\varphi_{ij}(1) = 0, \tag{C.4b}$$

$$\varphi_{ij}(2) = -\frac{25}{8}nk_B\frac{\mathscr{D}_{ij}}{x_i x_j}\sum_{k\in\mathscr{H}}\Lambda_{ik}^{01}\beta_{kj,1}(2), \tag{C.4c}$$

and for $\varphi_{ej},\ i \in \mathscr{H}$, by

$$\varphi_{ie}(1) = 0, \tag{C.5a}$$

$$\varphi_{ie}(2) = \frac{25}{4}nk_B\frac{\mathscr{D}_{ie}}{x_i x_e}\frac{\Lambda_{ee}^{01}\Lambda_{ie}^{01}}{\Lambda_{ee}^{11}}. \tag{C.5b}$$

References

[1] T.E. Magin, G. Degrez, Transport properties of partially ionized and unmagnetized plasmas, Phys. Rev. E (submitted for publication).
[2] A.F. Kolesnikov, The equations of motion of a multicomponent partially ionized two-temperature mixture of gases in an electromagnetic field with transport coefficients in higher approximations, Technical Report 1556, Institute of Mechanics, Moscow State University, Moscow, in Russian (March 1974).
[3] P. Degond, B. Lucquin-Desreux, Transport coefficients of plasmas and disparate mass binary gases, Transp. Theory Statist. Phys. 25 (1996) 595–633.
[4] S. Chapman, T.G. Cowling, The Mathematical Theory of Non-uniform Gases, second ed., University Press, Cambridge, 1960.
[5] J.H. Ferziger, H.G. Kaper, Mathematical Theory of Transport Processes in Gases, North-Holland, Amsterdam, London, 1972.
[6] J.O. Hirschfelder, C.F. Curtiss, R.B. Bird, Molecular Theory of Gases and Liquids, Wiley, New York, London, 1964, second printing, corrected, with notes added.
[7] C.R. Wilke, A viscosity equation for gas mixtures, J. Chem. Phys. 18 (4) (1950) 517–519.
[8] R.N. Gupta, J.M. Yos, R.A. Thompson, K.P. Lee, A review of reaction rates and thermodynamic and transport properties for an 11-species air model for chemical and thermal nonequilibrium calculations to 30,000 K, Technical Report, NASA RP-1232 (August 1990).
[9] J.S. Lee, P.J. Bobbitt, Transport properties at high temperature of CO_2–N_2–O_2–Ar gas mixtures for planetary entry applications, Technical Report, NASA TN D-5476 (November 1969).
[10] M. Capitelli, Simplified expressions for the calculation of the contribution of the heavy components to the transport coefficients of partially ionized gases, Z. Naturforsch. 27a (1972) 809–812.
[11] I.A. Sokolova, G.A. Tirskiy, Transport properties of gases and plasma mixtures for gas dynamics simulation, in: 32nd Thermophysics Conference, Atlanta, 1997, AIAA 97-2584.
[12] D.A. Copeland, New approximate formulas for viscosity and thermal conductivity of dilute gases, AIAA J. 41 (3) (2003) 525–537.
[13] G.E. Palmer, M.J. Wright, Comparisons of methods to compute high-temperature gas viscosity, J. Thermophys. Heat Transfer 17 (2) (2003) 232–239.
[14] A. Ern, V. Giovangigli, Fast and accurate multicomponent transport property evaluation, J. Comput. Phys. 120 (1995) 105–116.
[15] V. Giovangigli, B. Graille, Kinetic theory of partially ionized reactive gas mixtures, Physica A 327 (2003) 313–348.
[16] M. Capitelli, R. Celiberto, C. Gorse, A. Laricchiuta, P. Minelli, D. Pagano, Electronically excited states and transport properties of thermal plasmas: the reactive thermal conductivity, Phys. Rev. E 66 (2002) 016403.
[17] M. Capitelli, A. Laricchiuta, D. Pagano, P. Traversa, Electronically excited states and transport properties of thermal plasmas: the viscosity, Chem. Phys. Lett. 379 (2003) 490–494.
[18] A.F. Kolesnikov, General formulation of the multicomponent plasma transport equations, in: Fletcher et al. (Eds.), Physico-chemical Models for High Enthalpy and Plasma Flows, von Karman Institute for Fluid Dynamics, Rhode-Saint-Genèse, Belgium, 2002, VKI LS 2002-07.
[19] J.D. Ramshaw, Hydrodynamic theory of multicomponent diffusion and thermal diffusion in multitemperature gas mixtures, J. Nonequil. Thermo. 18 (2) (1993) 121–134.
[20] R. Devoto, Simplified expressions for the transport properties of ionized monoatomic gases, Phys. Fluids 10 (10) (1967) 2105–2112.
[21] A. Ern, V. Giovangigli, Multicomponent Transport Algorithms, Springer, Berlin, 1994.
[22] A. Ern, V. Giovangigli, Projected iterative algorithms with applications to multicomponent transport, Linear Algebra Appl. 250 (1997) 289–315.
[23] Y. Saad, M.H. Schultz, GMRES: a generalized minimal residual algorithm for solving nonsymmetric linear systems, SIAM J. Sci. Stat. Comput. 7 (3) (1986) 856–869.
[24] B. Fisher, Polynomial-based Iteration Methods for Symmetric Linear Systems, Wiley and Teubner, New York, 1996.
[25] B. Bottin, D. Vanden Abeele, M. Carbonaro, G. Degrez, G.S.R. Sarma, Thermodynamic and transport properties for inductive plasma modeling, J. Thermophys. Heat Transfer 13 (3) (1999) 343–350.
[26] M. Capitelli, G. Colonna, C. Gorse, A. D'Angola, Transport properties of high-temperature air in local thermodynamic equilibrium, Eur. Phys. J. D 11 (2000) 279–289.
[27] A.B. Murphy, Transport coefficients of air, argon–air, nitrogen–air, and oxygen–air plasmas, Plasma Chem. Plasma Process. 15 (2) (1995) 279–305.
[28] R.S. Brokaw, Thermal conductivity of gas mixtures in chemical equilibrium, J. Chem. Phys. 32 (4) (1960) 1005–1006.
[29] E.I. Asinovsky, A.V. Kirillin, E.P. Pakhomov, V.I. Shabashov, Experimental investigation of transport properties of low-temperature plasma by means of electric arc, IEEE Proc. 59 (4) (1971) 592–601.
[30] K. Sutton, P.A. Gnoffo, Multicomponent diffusion with application to computational aerothermodynamics, in: 7th Thermophysics and Heat Transfer Conference, Albuquerque, 1998, AIAA 98-2575.